

Tests of DES Charge Coupled Devices

Lluís Galbany i González



Treball de recerca del programa de Doctorat de Física de la Universitat Autònoma de Barcelona, realitzat per en Lluís Galbany i González sota la direcció del Dr. Ramon Miquel i Pascual, i del Dr. Manel Martínez i Rodríguez.

Bellaterra, Abril de 2008

El Dr. Ramon Miquel i Pascual professor d'investigació ICREA a l'Institut de Física d'Altes Energies (IFAE) i professor associat del Departament de Física de la Universitat Autònoma de Barcelona (UAB), i el Dr. Manel Martínez i Rodríguez, investigador catedràtic a l'Institut de Física d'Altes Energies (IFAE)

CERTIFIQUEN: Que la present memòria, que porta per títol: "Tests of DES Charge Coupled Devices", ha estat realitzada sota llur direcció per en Lluís Galbany i González i que constitueix el seu Treball de Recerca del programa de Doctorat de Física.

Bellaterra, Abril de 2008

Ramon Miquel i Pascual

Manel Martínez i Rodríguez

Sarve Bhavantu Sukhinah

Sarve Santu Niramayaah

Preface

This is the 3rd cycle review of my work done at *Institut de Física d'Altes Energies (IFAE)*, to achieve the *Suficiència Investigadora* qualification. I am working at IFAE since September 2006 as a doctorate student being part of the *Dark Energy Survey (DES)* group. IFAE, with *Institut d'Estudis Espacials de Catalunya (IEEC)* and *Centro de Investigaciones Energéticas, Medioambientales y Tecnológicas (CIEMAT)* form the DES Spanish consortium.

This review is organized as follows. Chapter 1 briefly describes the Dark Energy Survey project pointing its goals and the ways to achieve them. Also describe the four main techniques that DES will use, alone and in conjunction with the South Pole Telescope Sunyaev-Zel'dovich effect survey, to probe dark energy. Then I describe DECam, the camera the collaboration will build to perform the survey. Next, in chapter 2, I describe the laboratory set-up the measurements took place. I also summarize the optimization of the set-up and the measurements performed in order to fully characterize it. In chapter 3, I summarize what is a charge coupled device, writing about its history, its operation, and the functions it can perform. Continuing, I show all the tests I have done, explaining what is the aim of each one and how I have done them. Finally, in chapter 4, I propose some conclusions once the testing of the DES CCDs has been performed at DESLab. Also include two appendices: in appendix A, the error calculation of all the parameters measured in the tests is detailed; in appendix B, the document automatically generated after testing one CCD, with all the results and the plots of the tests, is attached.

Contents

Preface	i
1 The Dark Energy Survey (DES)	1
1.1 Science program	1
1.1.1 Dark energy	1
1.1.2 Techniques	3
1.2 DECam, the survey instrument	6
2 The SLAB	9
2.1 Optical system	10
2.1.1 Integrating Sphere Characterization. Uniformity studies	14
2.1.2 Photodiode as an intensity calibrator. Quantum efficiency	16
2.2 DES cube	18
2.3 Monsoon readout system	20
2.4 The PC control	21
3 The CCDs and the tests	23
3.1 DES CCDs	28
3.2 The tests	31
3.2.1 Output transfer gate test (<i>OTG</i>)	33
3.2.2 Photon transfer curve test (<i>PTC</i>)	36
3.2.3 Muons test (<i>MUON</i>)	38
3.2.4 Noise test (<i>NOISE</i>)	40
3.2.5 Charge transfer inefficiency test (<i>CTI</i>)	40
3.2.6 X-ray test (<i>XRAY</i>)	42
3.3 Short comment on the results	44
4 Conclusions	45
A Error calculation	47
A.1 OTG and VOTGSCAN tests	47

A.2 PTC test	48
A.3 CTI test	50
B Full test example	53
B.1 OTG	54
B.2 VOTGSCAN	55
B.3 PTC	56
B.4 CTI	58
B.4.1 H+	58
B.4.2 H-	60
B.4.3 V+	62
B.4.4 V-	64
B.5 NOISE	66
B.6 X-Ray exposure	67

Chapter 1

The Dark Energy Survey (DES)

The Dark Energy Survey (DES) Collaboration is an international project with the goal of carrying out an optical and near-infrared galaxy survey with the purpose of determining the dark energy and dark matter densities and the dark energy properties, characterized through the parameter w of its equation of state with great statistical precision (5%). Four independent techniques will be used: redshift distribution of galaxy clusters, weak gravitational lensing on large scales, evolution of galaxy clustering, and type-Ia supernova distances. These methods are doubly complementary: they are sensitive to different combinations of cosmological model parameters and are subjected to different systematical uncertainties. Furthermore, by deriving the four sets of results from the same data set with a common analysis framework, it will be possible to separate the effect of dark energy on the geometry of the universe from the effect on the growth of structure. Moreover we will obtain important cross checks of the systematic errors and thereby make a substantial and robust advance in the precision of dark energy properties measurements. The survey will image 5000 sq. deg of the South Galactic Cap reaching \sim 24th magnitude in the *griZY* bands of the Sloan Digital Sky Survey (SDSS) filter system [1], and will collect data of 300 million galaxies, 15000 galaxy clusters, and 1200 type-Ia supernovae (SNe). It will be carried out over a 5 year period, concentrated between September and February and beginning in September 2010, and it will be using a new 3 sq. deg CCD mosaic camera (DE-Cam) mounted at the prime focus of the 4 m Blanco telescope at Cerro Tololo Inter-American Observatory (CTIO) in Chile.

1.1 Science program

1.1.1 Dark energy

Since 1998 it is known that the expansion of the Universe is accelerating, even if gravitational attraction among ordinary matter restraints the expansion. Two groups independently [2, 3] came to this conclusion through observations of type-Ia SNe luminosities and redshifts. The distances of the high-redshift SNe Ia were, on average, 10% to 15% larger than expected in a low mass density Universe ($\Omega_M = 0.2$) without a cosmological constant. The conclusion is that a mysterious form of energy, dubbed *dark energy*, whose properties are basically unknown, is the dominant component of the universe at the current time, with 70 – 75% of all mass-energy. The main scientific aim of the collaboration is to determine the properties of the dark energy, by measuring the w parameter of its equation of state, the equation that relates its pressure

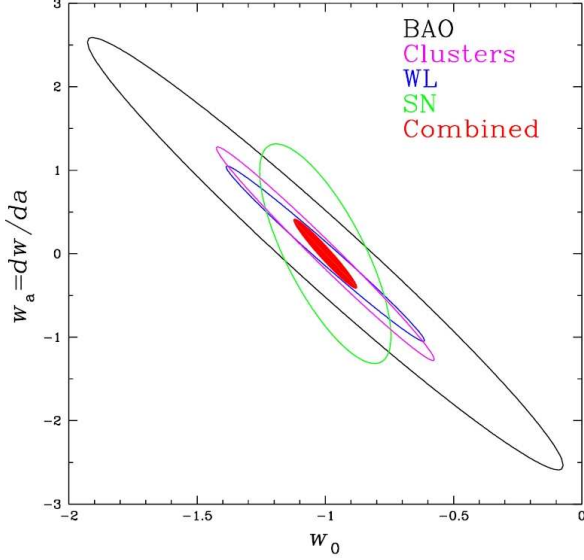


Figure 1.1: 68% CL forecast DES constraints in the $w_0 - w_a$ plane from the four probes of DES. The red region shows the constraint combining the four methods.

with its density ($p = w\rho$). If the dark energy turns out to be Einstein’s cosmological constant, then $w = -1$ everywhere at all times. However, in general, w may depend on cosmic time, or equivalently on redshift z . We can parametrize the redshift evolution of the dark energy equation of state by:

$$w(a) = w_0 + w_a(1 - a) \quad \text{where } a = \frac{1}{1+z} \quad (1.1)$$

then the w dependence on the redshift is:

$$w(z) = w_0 + w_a \frac{z}{1+z} \quad (1.2)$$

DES, through each of its techniques, will measure these three parameters related with w :

- w_0 , the equation of state now;
- $w_a = dw/da$, which measures the rate of change of w ;
- Ω_Λ , the dark energy density normalized to the critical density; the average density of matter in the universe today that would be needed exactly to halt, at some point in the future, the cosmic expansion. For a total density of the Universe equal to the critical density, the geometry of the Universe would be flat.

Combining the results of each technique we expect to be able to estimate the value of w (assumed constant) with a statistical precision of $\sim 5\%$. In Figure 1.1 we can see the forecast on the measurement of the w_0 and w_a parameters expected by each technique used in DES. One can also see the combined forecast constraints.

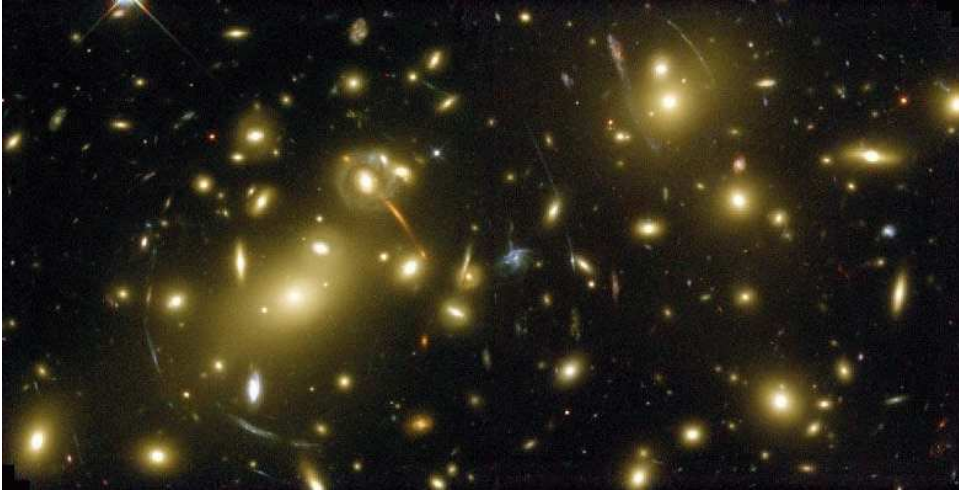


Figure 1.2: Galaxy Abell 2218's "Gravitational Lens" magnifies light of distant galaxies (image was taken by the Hubble Space Telescope)[4].

1.1.2 Techniques

DES aims at extracting cosmological information on dark energy from four different cosmological probes:

- *Galaxy clusters*

Galaxy clusters, the largest collapsed structures in the Universe, bears the marks of three influences: the spectrum of initial density perturbations, the physics of gravitational collapse, and the dynamically evolving spacetime. Then, their redshift distribution ($d^2N/dzd\Omega$) deliver precise constraints on the amount and nature of the dark energy. This distribution is the product of the comoving volume per unit redshift and solid angle ($d^2V/dzd\Omega$), and the comoving density of detected clusters (n_{com}).

$$\frac{d^2N}{dzd\Omega} = \frac{d^2V}{dzd\Omega} n_{com} = \frac{r^2}{dzd\Omega} \int_{M_{lim}}^{\infty} dM \frac{d^2n}{dVdM} \quad (1.3)$$

where $d^2n/dVdM$ is the galaxy cluster density mass function. From the observed galaxy clusters redshift distribution, we can study both the effect of the evolution of the volume element, related to the geometry of the Universe, and the effect of the evolution of the clusters mass function, related to the growth of density perturbations.

Another feature of the DES cluster survey is its complete coverage of the South Pole Telescope (SPT) Survey region. The SPT [5] will use the integrated Sunyaev-Zel'dovich effect (SZE) flux decrement, to identify galaxy clusters out to large distances, providing a census of tens of thousands of clusters over a 4000 sq. deg region south of declination $\delta = -30^\circ$, included in the survey region of DES. The DES is designed to measure efficiently and accurately photometric redshifts for all SPT clusters to $z = 1.3$. Existing cameras would require decades to cover the SPT survey area to the wished depth. Together, the DES and SPT offer unique adventages to precision cluster cosmology.

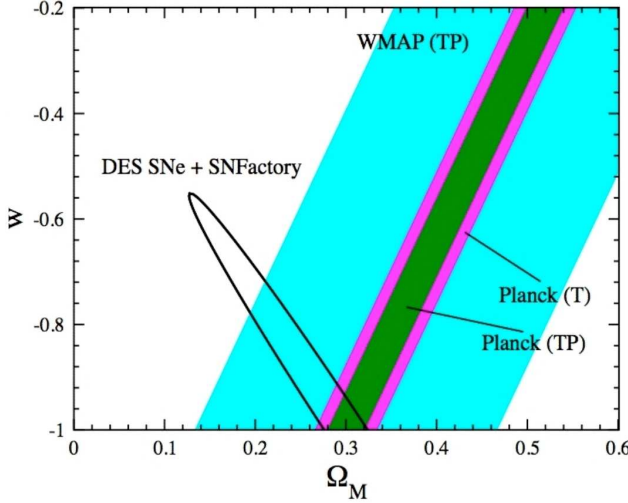


Figure 1.3: DES SN constraints and CMB constraints on the dark energy equation of state and dark matter density, assuming a flat Universe. SNFactory here denotes that a sample of 300 nearby SNe Ia are assumed to anchor the Hubble diagram at low redshift.

- *Weak lensing tomography*

The gravitational bending of light by massive structures in the Universe distorts the images of distant galaxies. These structures, such as galaxy clusters or dark matter halos, induce a coherent tangential shear pattern that can be used to reconstruct their surface mass densities. The evolution of the statistical pattern of WL distortions and of the cross-correlation between foreground structures and background galaxy shear, are sensitive to the cosmic expansion history through both geometry of the universe (radial distances) and the growth rate of structure (foreground mass distribution) [6, 7]. In the course of surveying 5000 sq. deg to the depth required for cluster photo- z 's, the DES will measure shapes and photometric redshifts for ~ 300 million galaxies and, with improved control of the optical image quality, enable accurate measurements of lensing by large-scale structures. In the Figure 1.2 it is shown an example of weak gravitational lensing, it can be seen how different stretched images appear around a brighter galaxy acting as a lens.

- *Supernovae luminosity distances*

In 1998, usage of low- and high-redshift type-Ia SNe as precision distance indicators provided the first direct evidence of the accelerating expansion of the Universe and of the existence of dark energy. Type-Ia SNe can be turned into cosmological standard candles through the relationship between their duration and luminosity (Phillips relation [8]). From ground-based telescopes, type-Ia SNe can provide luminosity distances up to redshifts around 1, with about 7% precision. The Hubble diagram (distance vs. redshift) measures the history of the expansion rate of the universe, which depends on the dark energy properties. In addition to the wide-area survey, the DES will use 10% of its allocated time to discover and measure well-sampled r , i and z light curves for about 1200 type-Ia supernovae in the redshift range $0.3 < z \sim 1$ through repeat imaging of a 9 sq. deg region,

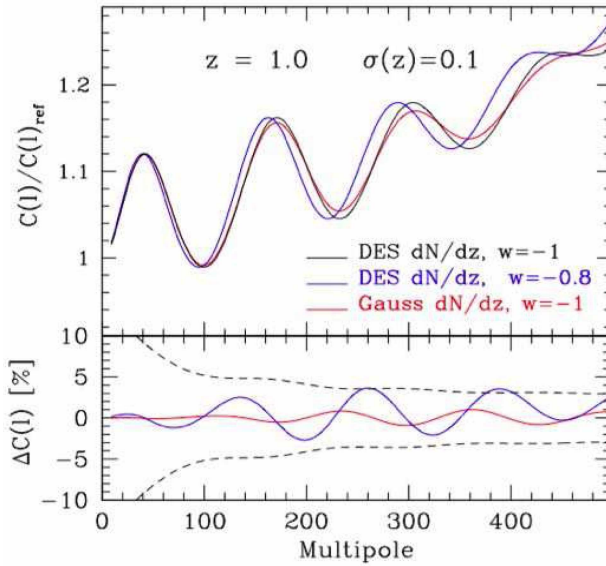


Figure 1.4: Top panel shows the angular baryonic acoustic oscillations for a redshift slice of thickness $\Delta z = 0.1$ at $z = 1$, calculated by dividing the non-linear angular power spectrum C_l for $w = 1$ (black) and $w = 0.8$ (blue) by a linear theory model with no BAO. The red curve shows the effect on the BAO signal in the $w = 1$ case when using photo-zs with standard deviation of $\sigma_z = 0.05$ per galaxy. Bottom panel shows statistical errors for DES in multipole bins of $\Delta l = 30$ (dashed lines), compared to the percentage differences of the blue and red curves of the top panel from the fiducial (black) model.

with a cadence of 5 visits per lunation. These SNe will provide relative distance estimates to constrain the properties of the dark energy. In figure 1.3 it can be seen the constraints on the dark energy equation of state parameter w , and dark matter density ΩM .

- *Galaxy angular clustering*

The DES will measure the angular clustering of galaxies in photometric redshift shells out to $z \sim 1.1$. The matter power spectrum as a function of wavenumber shows characteristic features, a broad peak as well as baryon wiggles arising from the same acoustic oscillations that give rise to the Doppler peaks in the Cosmic Microwave Background (CMB) power spectrum; these features were recently detected in the SDSS [9] and 2dF. These oscillations of the coupled photon-baryon fluid in the early Universe imprint a “standard ruler” scale on the pattern of matter clustering. This baryon acoustic oscillation (BAO) scale, set by the sound horizon scale at the epoch of recombination, can be calculated from straightforward physics and calibrated by its projection in the CMB, providing a geometric test of cosmological parameters. The predicted angular power spectrum in a redshift slice of width $\Delta z = 0.1$ centered at $z = 1$ is shown figure 1.4.

In addition to these methods, cross-correlation of CMB data sets with DES galaxies as tracers of potential wells will probe the dark energy through the temperature anisotropies across the line of sight (Integrated Sachs-Wolfe effect, ISW [10]). Finally, we note that accurate photometric redshifts are critical to the DES science goals; as a relatively shallow survey, a major advantage of the DES will be the availability of spectroscopic redshift calibration (training) samples that will extend out to the flux limit of the survey.

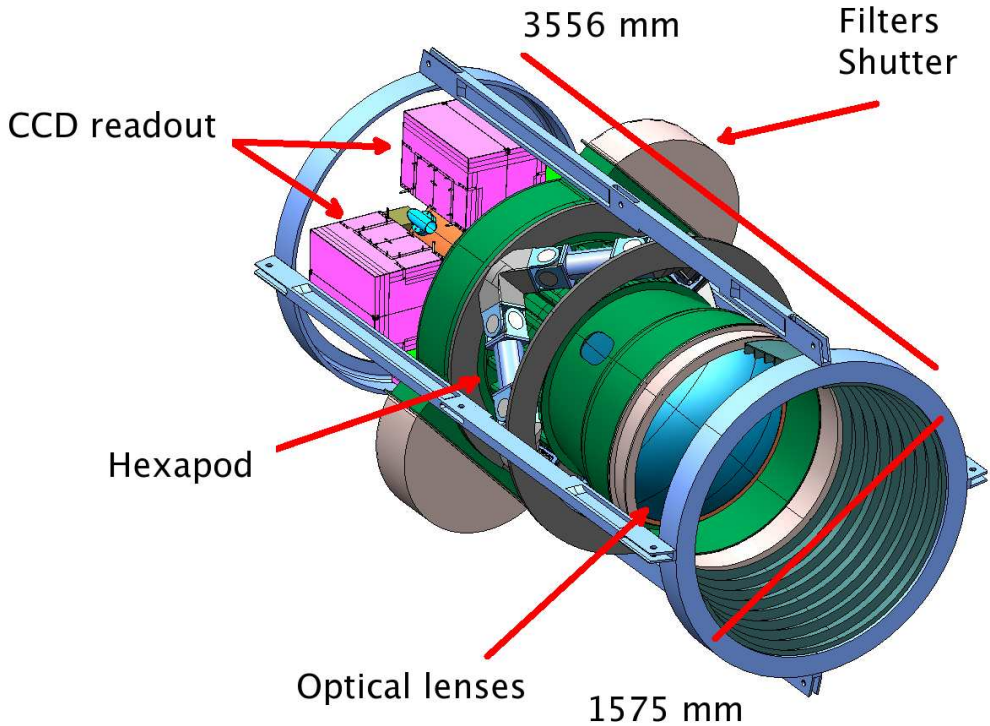


Figure 1.5: DECam reference design, where its major parts are pointed out.

1.2 DECam, the survey instrument

The philosophy of the DECam project is to assemble proven technologies into a powerful survey instrument and mount the instrument on the optimally configured Blanco telescope, thereby exploiting an excellent, existing facility. DECam will be installed in a new prime focus cage on Blanco. Figure 1.5 shows a schematic view of DECam with the key elements identified.

The major components of DECam are a 519 megapixel optical mosaic CCD camera and guide and focus sensors mounted on the focal plane, a five element wide-field optical corrector (2.2 deg \varnothing field of view), the Front End Electronics (FEE) system composed of a low-noise CCD readout system housed in actively cooled crates, a 5-band filter system with SDSS gri, and Z and Y filters plus three slots for additional filters, a cryogenic cooling system to maintain the focal plane at 180 K, an hexapod supporting the imager and corrector barrels providing lateral adjustability as well as focus control, and the Survey Image System Process Integration (SISPI), a data acquisition and instrument control system to connect to the Blanco observatory infrastructure.

The camera focal plane will consist of sixty-two 2046 \times 4096 CCD modules (0.27" /pixel) arranged in a hexagonal sensor covering an imaging area of 3 sq. deg. Smaller format CCDs for guiding and focusing will be located at the edges of the focal plane. To efficiently obtain infrared-band images for high-redshift ($z > 1$) galaxies, the fully depleted, high-resistivity, 250 μm thick silicon devices that were designed and developed at the Lawrence Berkeley National Laboratory (LBNL) [11] were selected. The thickness of the LBNL design has two important implications

for DES: fringing is eliminated, and the Quantum Efficiency (QE) of these devices is greater than 50% in the near-infrared wavelenghts (z band, 825-1100 μm), a factor of ~ 10 higher than traditional thinned astronomical devices. These CCDs also have 15 μm pixels, 2 readout channels per device, and a readout time of about 17 s ($< 10\text{e}^-$ readout noise). All these features make the CCDs a key component of the project.

The optical system design consists of five fused silica lenses that produce an unvignetted 2.2 deg diameter image area, which is calculated to contribute less than 0.4" FWHM to the point-spread function. The first element, the largest, has an optical clear diameter of 0.95 m. Two of the surfaces are aspheric: the concave surface of second element and the convex surface of the fourth one. The spacing between the third and the fourth elements will allow the shutter and the stacked filter changer to individually flip the filters in and out of the optical path. The fifth element is the window on the CCD vacuum vessel.

The Monsoon CCD readout system developed by the National Optical Astronomy Observatory (NOAO) has been adopted. It consists of 3 boards: the Master Control Board (MCB), the Clock & Bias Board (CBB) and the Data Acquisition Board (ACQ). DES has made some improvements to reduce the final volume of the system. DES modifications include high-density (12 channels) ACQ, a simplified Clock Board (CB) - the same CBB but without bias outputs and with more clock outputs - and a re-designed MCB incorporating S-Link optical data transfer. UIUC, Fermilab and IEEC-IFAE each have a Monsoon system and are able to read out LBNL CCDs and make some tests to assess whether these CCDs and their electronics meet the requirements of the project. As we gain experience with Monsoon in the test setups, we will further develop on the design and make the modifications needed to meet the prime focus cage space and heat restrictions.

IFAE, as part of Spain-DES Collaboration (altogether with IEEC and CIEMAT), will make significant in-kind contributions to the testing of the focal plane detectors; the DECam telescope guider, which is part of SISPI; the Survey Planning; and the Front End Electronics. The FFE contributions include the design, fabrication and testing of the prototype and production versions of the Master Control Board, the Clock Board and their transition cards; and the development and provision of an S-Link optical readout for the Monsoon systems to replace the less supportable Systran fiber links.

Chapter 2

The SLAB

The SLAB is the place where all the measurements related with the DES project are physically performed in IFAE. We were looking for a name to be given to this facility and, by tricking the name "DES lab", we were thinking about "The SLAB", which also means "Study of Light on vibro-Attenuated Bench". It consists basically of a wide table furnished with all the devices needed to correctly perform our activities. This table, as can be seen in the figure 2.1, hosts the optical system that provides uniform light of precise wavelength to the CCDs and its controlling instruments, the nitrogen container, the vacuum pump, the dewar that contains the CCD cooled and in vacuum conditions, the Monsoon readout system, and two computers that centralize all the measurements through GPIB, Serial and Parallel connections.



Figure 2.1: The SLAB. One can see the optical system and the devices controlling its parts, the DES cube, the N_2 container, the vacuum pump, the Monsoon readout system and the computers.

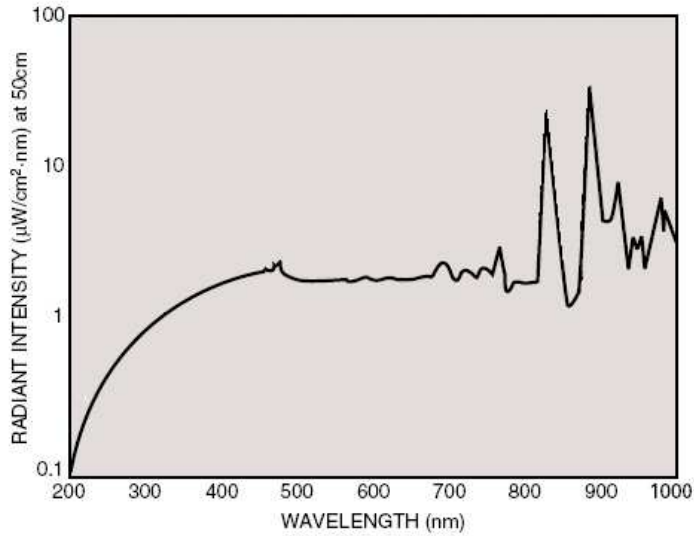


Figure 2.2: Spectrum of the Xe lamp provided by the manufacturer.

2.1 Optical system

The optical system allows us to control what kind of light arrives at the CCD to provide flat field images for tests. It consists of a *Xe* lamp, a system of three lenses to focus the light beam, a filter wheel to cut unwanted wavelengths, a monochromator to select a desired wavelength, an electro-mechanical shutter that controls the exposure time, a 6 inches integrating sphere that collects the incoming light and produces a uniform parallel beam, a baffle that keeps isolated the beam up to the dewar, and a photodiode to monitor the intensity of the light arriving to the CCD.

- *Xe* lamp

The lamp used on the SLAB is the *Xe* L2274 model from Hamamatsu. It is an arc lamp of 150 W, with a short-gap between the two electrodes, and an ozone-free silica bulb. The arc is 2 mm long and the spectral distribution of the emitted light goes from 220 to 2000 nm. The Figure 2.2 shows the entire emission spectrum of this lamp.

- Focusing optical system

The focusing optical system is used to converge the light from the *Xe* lamp into the entrance slit of the monochromator. This light has to satisfy two main requirements: it has to be as much as possible and the beam has to be formed by parallel rays. It can be achieved with some optical lenses. The first requirement was satisfied by putting a lens of small focal length, $f_1 = 40$ mm, right at this distance from the *Xe* lamp arc. In this way, most of the light from the lamp is captured. Next, a second lens of focal length $f_2 = 75$ mm makes the rays converge into a diaphragm, located at 7.5 cm from this second lens. The image generated by this lens in its focal plane is point-like, making it better because it is smaller than the original image of the arc lamp. The diaphragm is used to let the arc image alone pass to the third lens, therefore reducing the contribution of stray

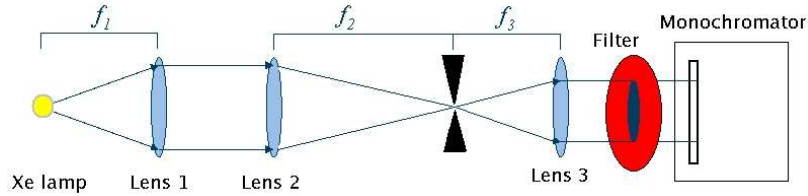


Figure 2.3: The optical configuration.

light. Finally, at 4 cm from the diaphragm, a lens of focal length $f_3 = 40$ mm is placed in order to render again parallel the light beam and to enter it in the monochromator slit.

- Filter wheel

The light exiting the last lens contains all the wavelengths emitted by the Xe lamp, from 220 to 2000 nm. If this light were fed directly to the monochromator then, for any given wavelength λ_0 , we would also have the contributions of all the submultiple wavelengths of λ_0 , according to the formula:

$$\lambda_n = \frac{\lambda_0}{(n + 1)} \quad (2.1)$$

with n order of diffraction, going from 1 to ∞ . In order to avoid all the undesirable wavelengths, the beam must be cut above the first diffraction order λ_1 . In fact, all the further diffraction orders will have wavelengths smaller than the first one, and will therefore be cut off by a high-pass filter already cutting λ_1 .

For the purpose of the DES project, the wavelengths of interest for the characterization of the CCDs will range between ~ 300 and 1200 nm (indeed, only the wavelengths between 400 and 1100 nm will be observed, but a margin of 100 nm on both spectrum edges is desirable to further study the CCDs behavior). Based on this assumption, a set of three high-pass (in terms of wavelength) filters is enough to fully characterize the CCDs. The minimum wavelength the filter allow to pass, and the rang of wavelengths used for each one, are shown in Table 2.1.

Although these are the true transmission bands, we only use the WG-295 filter to analyze light from 300 to 450 nm, the GG-400 from 400 to 750 nm, and RG-665 from 700 to 1200 nm. With these three filters we are able to cover the entire spectral range of interest, without any higher diffraction order entering the monochromator.

Table 2.1: Minimum wavelength for the high-pass filters being used on the SLAB. The range used for each filter is selected in order that the second diffraction orders do not enter the monochromator.

Filter	Min. λ (nm)	Rang λ used (nm)
WG-295	265	300-450
GG-400	380	400-750
RG-665	620	700-1200

- Monochromator

A monochromator is used to select the wavelength being used for the measurements. The device we use on the SLAB is a Digikröm CM110 from Spectral Products.

The device allows to scan from 200 to 1600 nm by properly selecting one of two diffraction gratings hosted within the device. The efficiency of the device depends on the incoming wavelength. The device provides an accuracy in wavelength of ± 0.6 nm, and can be driven either via a cabled remote control or a serial port. In the latter case, the control of the device can be given to automated software packages developed with the National Instruments LabView platform. The bandpass of the exiting light can be chosen between 1 and 16 nm by inserting the suitable set of slits at both the input and output port of the device. For our purposes most of the measurements were made with slits with bandpass of 4 nm, and at every 5 nm.

- Electro-mechanical shutter

At the output of the monochromator it is installed an electromechanical shutter which is used to cut the light entering the integrating sphere and to control the exposure time. The device is very simple in concept, design and realization, as it is simply made by an electromagnet pushing/pulling a thin metal sheet over the light beam, thus intercepting it. Its most interesting feature is the possibility to set its status (open/closed) it via a TTL input signal. In practice, this feature allows to take dark measurements as close as possible to the measurements with light, without the need to switch on and off the lamp. The shutter is controlled via one of the bits in the parallel port of a PC with LabView. With this set-up we performed a series of measurements in order to evaluate the minimum achievable shutter time, which came out to be 10 ms.

- Integrating sphere

An integrating sphere is a device used to render uniform a beam of light. In DES lab, it is used to flat out the pencil of monochromatic light getting out of the monochromator. The device we use on the SLAB is a 6 inches model M-70674 from Oriel, with three ports of 1.5 inches, and inner coating made of $BaSO_4$. Its reflection response is shown in figure

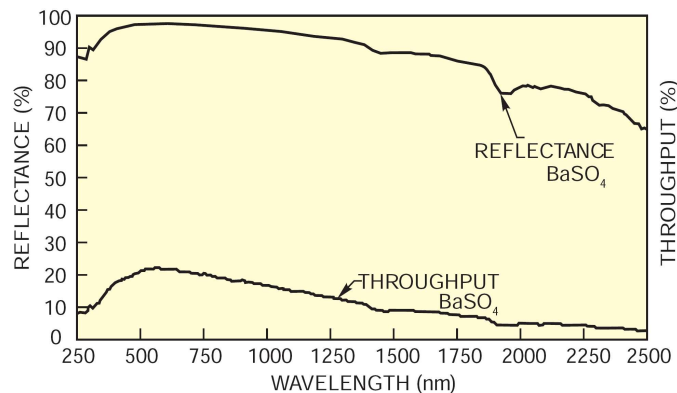


Figure 2.4: The reflectance and the throughput of the integrating sphere, as a function of the wavelength.

2.4. We have connected one port to the shutter, another facing the CCD, and we have covered the last one.

- Baffle

After some tests described below (3.1.1), the distance between the sphere output port and the CCD plane was set at 13 inches. This means that there is some open space between the integrating sphere output port and the cube hosting the CCD. Some unwanted light might therefore enter the cube, were not for an optical baffle between the sphere and the cube. This device, resembling a daguerreotype, is made of black, smooth plastic, and should prevent both the external light to enter the cube and the internal light to be reflected in odd ways.

- Monitoring photodiode

In order to perform measurements with the CCDs calibrated in number of photons, light intensity, etc., a photosensitive device well calibrated to be used as a reference was needed. For this purpose we used a silicon photodiode from Hamamatsu, type S1337-1010BQ. Its sensitivity ranges from 190 to almost 1200 nm, thus covering the spectral range of interest for our application.

In order to cut on the electronic noise sources, it is good to put a preamplifier stage as close as possible to the measuring device. The gain of this stage is usually of no concern, ideally it should be unitary, as its purpose is not to make the signal bigger, but to make it more insensitive to noises usually induced on the long wires going from the measuring device to the read-out apparatus. Very close to our photodiode, we have a pre-amplifier stage made at Max-Planck Institute in Munich, whose gain can be set either at 10 or 100 pA/mV. Usually, our measurements are taken in the first of the two conversion modes.

The final stage of the photodiode chain is the Keithley 2700 multimeter being used for the read-out of the light intensity. The device features a resolution of 22 bits (6.5 digits), and it is controlled with various LabView applets through the GPIB port.

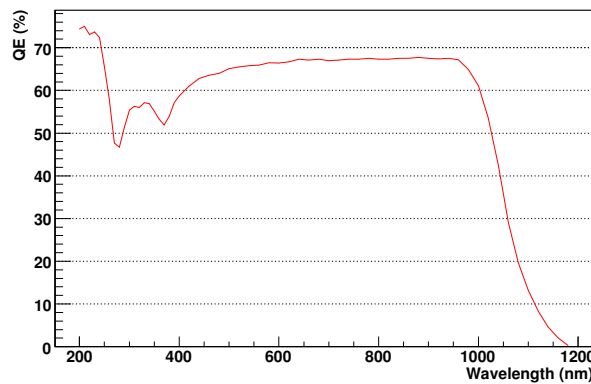


Figure 2.5: The QE of the photodiode

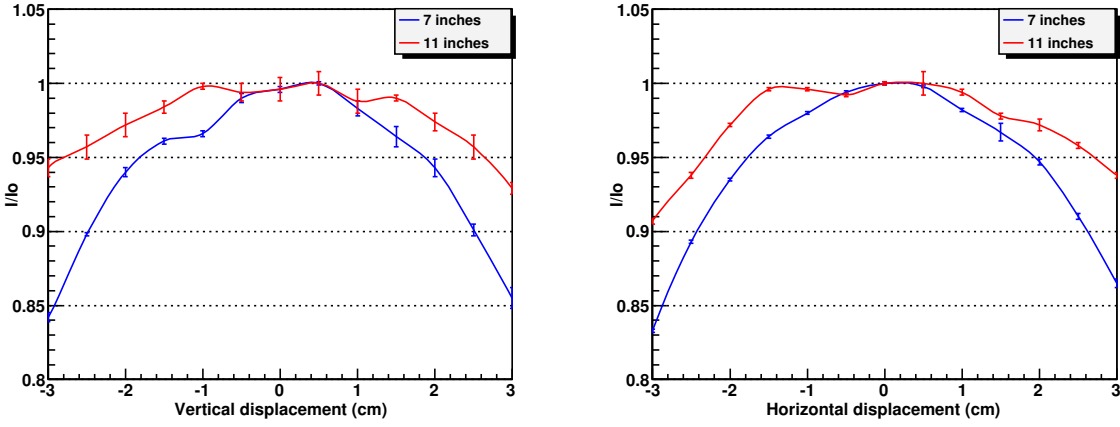


Figure 2.6: Here we can see the uniformity at 11 inches from the sphere output port to be better than at 7 inches. On the left side, the results of the vertical scan, and the horizontal ones on the right side. The jitters are due to the manual displacement of the photodiode support.

2.1.1 Integrating Sphere Characterization. Uniformity studies

Distance between sphere and CCD

Before testing any CCD, we have to characterize the light we are going to use to carry out these tests. In the preliminary studies we want to know how the intensity of the light emitted by the integrating sphere decreases with the distance from the beam axis. It will help us to decide at which distance we will put the CCD to perform the tests.

According to the integrating sphere technical guide [12], the uniformity of the output beam of these devices gets better with the distance from the sphere itself. The area of a sphere of a few inches in diameter is more curved than the same area of a larger one. In the guide it is defined the irradiance as the flux density falling on a surface measured at the plane of the surface. Then, the irradiance over a plane intercepting the light beam follows the law:

$$I(x, y) = I_0 \cos^4(\theta) \quad (2.2)$$

I_0 being the axial irradiance and θ the angle at the sphere port between the axis of the light beam and the direction pointing to (x, y) . This equation holds true for small values of θ ($< 10^\circ$),

Table 2.2: Irradiance uniformity (I/I_0) at different distances from the beam axis. The results are the mean of the vertical and the horizontal scans. x is the distance from the sphere to the photodiode. d is the displacement of the photodiode from the beam axis.

x (in)	$d = -3$ cm	-2 cm	-1 cm	0 cm	1 cm	2 cm	3 cm
7	0.84	0.94	0.98	1.00	0.98	0.94	0.86
11	0.93	0.97	0.99	1.00	0.98	0.97	0.94
14	0.96	0.97	0.99	1.00	0.99	0.97	0.96

and gives an approximated value for the true irradiance in the point (x, y) of a plane in front of the sphere output port.

In order to perform these measurements, we tried to put the Hamamatsu photodiode at different distances from the output port of the integrating sphere, and then took measurements over 6 cm transversally to the light beam at every 5 mm. This means that for each distance we have performed two measurements: a vertical and a horizontal one. It has to be taken into account that the movement of the photodiode support was performed manually, although we had a mechanic guideline that allows us to take measurements every 5 mm approximately. The results at 7 inches and at 11 inches are shown in Figure 2.6 and more explicitly in Table 2.2 with the 14 inches ones.

From the results we can get the conclusion that the farther we put the photodiode, the better the uniformity is, as we already knew. But as in Fermilab, where they also have to perform the same tests that we do, they put the CCD at 13 inches from the sphere output port, we have finally decided to carry out the tests at 13 inches like them. At this distance we achieve more than 99% of irradiance in the first centimeter away from the beam axis. This decision will also allow us to compare our results because the uniformity has to be similar.

Uniformity maps

Once we have decided how far we will put the CCD, the next step to improve our studies on the characterization of the integrating sphere outgoing light, is to draw the whole intensity surface at this distance. It will allow us to know the response of each CCD pixel separately. We can take an image with a CCD at 13 inches and plot this image as a luminosity surface. The image is expected to have the same curvature on this surface than in the photodiode one, but might there be some discrepancies. The normalization of the two surfaces gives us the real behavior of each pixel.

In order to use the photodiode to collect these uniformity maps, it was necessary to move it along the plane of the CCD, transversally to the beam axis. Therefore an X-Z holder was built to move the photodiode by means of two stepping motors. These motors are moved in both directions by a LabView application and controlled through the parallel port.

We planned to scan a square surface of $6.2 \text{ cm} \times 6.2 \text{ cm}$ with a step of 2 mm, in this way we have 32×32 different positions where we can take data. Beginning from the low left end we have read the first horizontal row, then we have raised a step up, and we have read from right to left side the second horizontal row. This way up to finish in the top left end. In order to have readings of all the spectrum we have used the three highpass filters mentioned before: one from 300 to 450 nm, a second one from 400 to 750 nm and a third one from 700 to 1200 nm. We have made the readings with changing the selection of wavelength of the monochromator each 5 nm. For each position we have one reading *before* without light (with shutter closed), one reading of the spectrum (with light) and one reading *after* without light. That is, for example, for the point $X00 - Y00$ we have 9 files: 1 before, 1 reading and 1 after for each filter. Finally we have 9216 files with the data of the intensity of the light that arrives at 13 inches of the sphere.

In the *before* files as well as in the *after* ones, there are ten readings of intensity in order to make a linear regression of the variation, since there should not be any. Then in the *before* files we have taken the last point of the regression, while in the *after* we take the first one. These will be the extreme points of the electronic noise pedestal that we will subtract to our reading, adjusting them to a straight line in order to take into account the variation with time of the

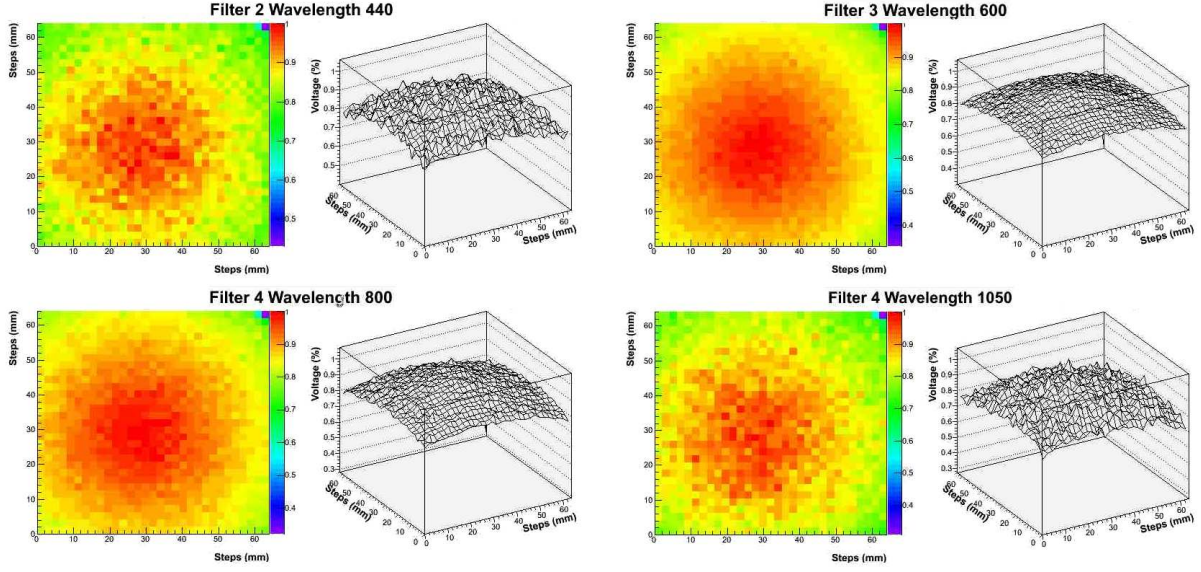


Figure 2.7: Uniformity map at different wavelengths. Every point is normalized to the center value. It is easy to see the variation in the curvature among the surfaces.

pedestal from the beginning of the reading until the end.

In the files with the light measurement data, there are the intensity readings for each wavelength that leaves the monochromator. With these 3072 files, after subtracting the pedestal, we can reconstruct the $6\text{cm} \times 6\text{cm}$ uniformity maps of our Xe lamp for multiple wavelengths from 300 to 1200 nm, at every 5 nm.

After analyzing the results we have realized that the curvature of the uniformity surface varies with the wavelength, as we can see in Figure 2.7. This fact is not a problem for our purpose, because we only want to know the curvature of each wavelength, in order to normalize with the corresponding CCD irradiance surface. However, from this result we can get that the reflectant material of the sphere integrates better some wavelengths. This can be due both to the response of the BaSO_4 to different wavelengths, and the particular spectrum of the Xe lamp.

2.1.2 Photodiode as an intensity calibrator. Quantum efficiency

The photodiode can be even more useful than it was up to now. As the photodiode is calibrated from factory in number of photons of a given wavelength per picoamper, we can also use it to measure the quantum efficiency (QE) of our CCD. The QE is the ratio between the number of photons interacting with the silicon atoms of the CCD and the number of photons arriving at the CCD. When the QE is equal to one, it means that all the photons interact with the detector.

The first step to measure the QE would be to know the intensity loss between the light exiting the sphere and the light arriving at the CCD. We can measure the intensity spectrum at the pinhole output of the integrating sphere, and then make the same measurement at the CCD plane (13 inches). In fact we can also take the central value of the uniformity surfaces used before. In the case that there is no spectral dependency of the intensity, then the ratio:

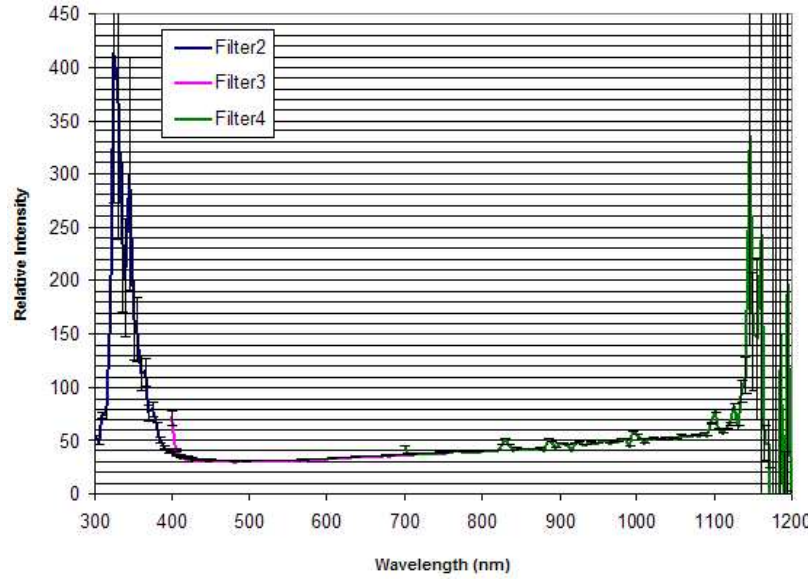


Figure 2.8: Ratio of the intensity measured with the photodiode at the output port of the sphere and at 13 inches from it, for all possible wavelengths. We can see that at 400 nm the intensity at the output port is 30 times larger than at the CCD plane, while at 1100 nm this ratio is up to 60. [13]

$$R(\nu) = \frac{I_P(\nu)}{I_{CCD}(\nu)} \quad (2.3)$$

with $I_P(\nu)$ the intensity at the pinhole output and $I_{CCD}(\nu)$ the intensity at the CCD plane, is a constant. Nonetheless, as one can see in the Figure 2.8, this function was found to be not a constant. Apart from the head and the tail of the graph, where big errors apply due to the very small lamp emission, from 400 to 1100 nm one can observe a steadily, rising slope in the $R(\nu)$ graph. It is the same effect already described: the inner coating material of the sphere integrates differently the light depending on its wavelength. Although we already knew this fact, this first measurement is useful because later on we will have to take into account this $R(\nu)$ factor, when measuring the QE for each wavelength.

As described in the next chapter, one of the tests we want to carry out on the CCDs is the gain test, which is done to evaluate how many electronic counts (Analogic to Digital Units, ADU) the amplifier produces per electron. The result of this test is a relation between electrons and ADUs. On the other side, clearly that the number of electrons from an atom that are pulled out by a photon interacting with the atom, depends on the energy of the photon and on the kind of atom. For silicon, with an energy gap of 1,14 eV, photons of energy from this to 3.1 eV (400 to 1100 nm) can only pull out one electron. Photons with more energy pull out more than one electron but, fortunately, this energy range is the one we are interested in and the one we work with. Then we can suppose that 1γ generates $1e^-$.

This result altogether with the relation between electrons and ADUs gives us the relation photons/ADUs. With this, we can calculate the number of interacting photons (p_{int}) taking the number of ADUs of the center pixel of the CCD.

Once we have made all the relations we could achieve the measurement of the QE placing the

photodiode in the port of the sphere opposite to where the baffle is connected. For this purpose, we have made a small hole in the tap where the photodiode is put, in order to avoid external light entering. Then, while we are taking an image, the photodiode tells us the intensity exiting the sphere simultaneously. We can convert the number of electronic counts in the center pixel of the image to interacting photons. Taking the measure of the photodiode at the exit of the port (p_0) we can calculate the QE:

$$QE = \frac{p_{int}}{p_0 \times R(v)} \quad (2.4)$$

where we have used the factor depending on the wavelength explained above.

Measuring the intensity with the photodiode at the same time that the image is taken, makes the result better because the two measurements are taken in the same conditions.

2.2 DES cube

The CCD must be cooled and enclosed inside a device where the vacuum can be produced, and where only the selected light could arrive to it, in order to perform our tests. At the end of the optical system described before, we connect the baffle to an aluminum and copper cube prepared to satisfy all these conditions. This device was designed at Fermilab and, after some changes, was produced at IFAE in Barcelona, and at CIEMAT in Madrid.

As we can see in Figure 2.9, one of the walls of the cube was built with a circular glass window and an adapter to connect to the baffle end. This wall is held by four clamps and can

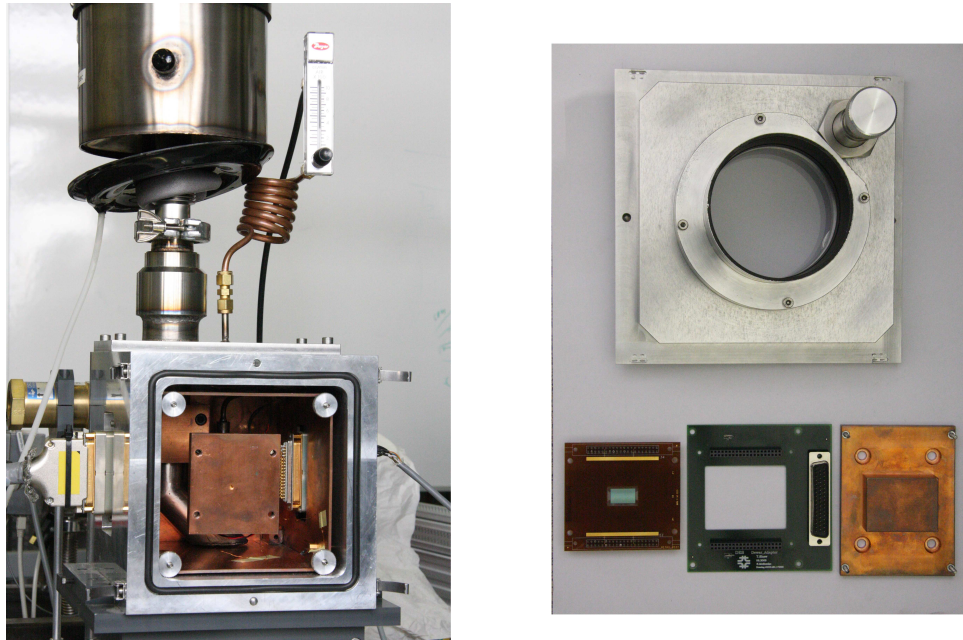


Figure 2.9: The DES cube. On the left photograph, it can be seen the copper box inside the aluminum one. The N_2 container is above the cube and finishes in a pipe where the N_2 enters inside the cube. There are two connectors on each side: one for the temperature and heater controller, and another for the readout of the CCD. On the right, there is the copper plate where an electronic readout board and the CCD sit.

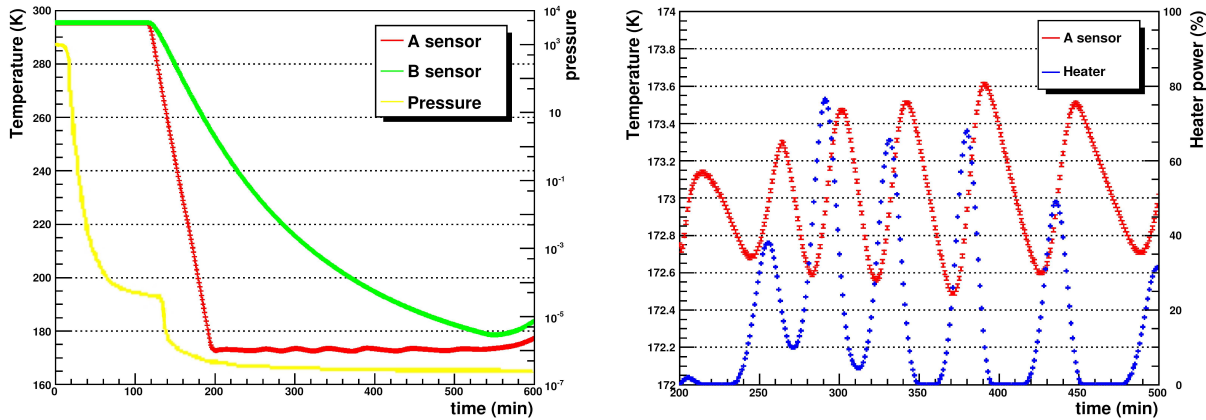


Figure 2.10: On the left, the temperature measured by the two sensors: A on the copper plate where the CCD is, and B on the copper box. The pressure inside the cube is also plotted. On the right, the stabilization of the temperature on the CCD. When the sensor detects the CCD is colder than the setpoint, the Lakeshore controller turns on the heater, and when the temperature increases the heater is disconnected.

be removed easily, in order to exchange the CCD in a very handy way. Above the cube there is a deposit where we manually put the liquid N_2 in order to cool the interior. The N_2 allows us to cool down to 77 K, its boiling point. The exterior walls of the cube are made of aluminum and inside there is a copper box designed to isolate the cold parts from the exterior walls. The deposit ends in a copper pipe that goes through the cube and the copper box. Then a smaller diameter pipe is used to vent the evaporated nitrogen that leaves the cube. The pipe connects to a valve that controls the gas flow. The front copper box plate where the CCD sits, is cooled by thermal diffusion from the pipe because there is no contact between the N_2 and the other parts of the cube.

The vacuum system consists of a turbomolecular pump and a diaphragm pump. The diaphragm pump is connected to the turbomolecular pump which is already connected to the back of the cube through a flexible hose. There is also a vacuum gauge and a safety relief valve in case of a leak of N_2 inside the cube. This vacuum system has a display control unit which controls all the pumps and measures the vacuum value inside the cube.

The time expected to produce a vacuum better than 1×10^{-5} mbar is 1.5 hours. When this value is achieved, the N_2 can be loaded into the deposit. We must open the flow control valve to increase the velocity flow of the liquid which will cool down more efficiently. The turbomolecular pump is kept working to remove the condensed air. In approximately another hour and a half, the temperature 173 K is achieved on the copper plate, and the pressure keeps decreasing down to approximately 1×10^{-6} mbar. In Figure 2.10 the evolution of the temperature and the pressure inside the cube is shown. In the right side it is also plotted how the Lakeshore controller (described below) switches on the heater when the temperature is decreasing, in order to stabilize the temperature at the setpoint.

If we do not do anything, the temperature keeps decreasing down to 77 K. We need to stabilize it at the selected temperature of 173 K, at which will be the camera in the Blanco telescope. For this we use the Model 332 Lakeshore temperature controller. This controller is connected to two sensors, one at the back of the copper box and another at the back of the CCD plate. It also has a resistance of 25Ω used as a heater. The Lakeshore uses a proportional-

integral-derivative (PID) control algorithm to calculate when it has to provide intensity to the resistance heater in order to keep the temperature at the place where the sensor is put at the selected setpoint. The sensor placed near the CCD detects lower temperature than the other. As time goes by, the temperatures in both sensors will approximate and reduce the fluctuations.

At this point, with the temperature and vacuum wanted, we can begin to take the data of the CCD images.

2.3 Monsoon readout system

The data from the CCD is collected by an electronic readout system called Monsoon. It has been developed by NOAO, but the DES project has made some changes in order to make it more compact and light. The Monsoon readout system is housed in a crate where there are the three types of boards: the Master Control Board (MCB), the Clock Board (CB) and the Data Acquisition Board (ACQ). The complete system is shown in Figure 2.11.

The Master Control Board is the system interface. It controls all backplane functions, such as reading and writing to registers, as well as controlling the readout of the CCDs. It communicates with the control computer through an optical fiber. Up to now, in Fermilab, the Systran system is used to communicate Monsoon with the host computer, but after study by DES-Spain, it has been decided to use instead the S-Link system, an open source communication link that has



Figure 2.11: The Monsoon readout system: the three boards (from top to bottom: ACQ, CBB, MCB) inside a crate. The S-Link board integrated in the MCB can be seen. The connection between the MCB and the computer is done by optical fiber.

long been used at CERN.

The Clock Board provides 32 clock outputs and 40 bias outputs. This board is being designed at CIEMAT to be able to provide many more clock outputs. The bias control of the previous version of the board (Clock & Bias Board, CBB), has been moved to the ACQ board. The new one would service up to nine CCDs, whereas the current only supports two.

The Acquisition Board provides eight channels to digitize the CCD video outputs as well as 32 Bias Voltages. This board is being redesigned in order to suit the DES needs and reduce the number of overall boards required by the DECam system. Thus, Fermilab has designed and tested a new Acquisition Board with 12 channels that provides bias voltages for six CCDs, instead of the four the 8-channel could read. In any case, in the test step, we only read one CCD at a time, and then we only would need two channels, one for each side of the CCD.

The pixel data of the CCD is read by two amplifiers, one for the right half and another for the left side, transforming the counts of the pixels to electric signal. A cable transports these signals to the right side wall of the cube, where using a connector, another wire brings the information to the Monsoon boards.

2.4 The PC control

The images are taken with *MecStart*, the Linux program that controls the Monsoon system. *MecStart* talks with the Monsoon Pixel Acquisition Node (PAN) on the MCB via network sockets and can change the voltages, change the clocks, make a reading of the CCD, open or close the shutter... and all the features Monsoon is able to perform. It needs an input file where all the initial voltages used by Monsoon are typed in. It also loads another file where we have written the sequence of orders Monsoon has to do in order to take the images required for every test. This file is based on the Tcl/tk (Tool Command Language combined with ToolKit extension for Tcl) scripting language.

A Labview virtual instrument (VI) [14] has been programmed in order to control all the devices of the optical bench instruments. Our VI saves a log of all the actions done by the user to the optical system instruments. It can change the wavelength the monochromator selects, move the filter this wavelength needs, open and close the shutter if the user wants to take an image, switch on the remote control of the Lakeshore temperature controller and visualize and save the temperature of the sensors, program the displacement of the photodiode motors, and save and visualize the intensity lecture of the photodiode. In Figure 2.12 the front panel of the VI is shown.

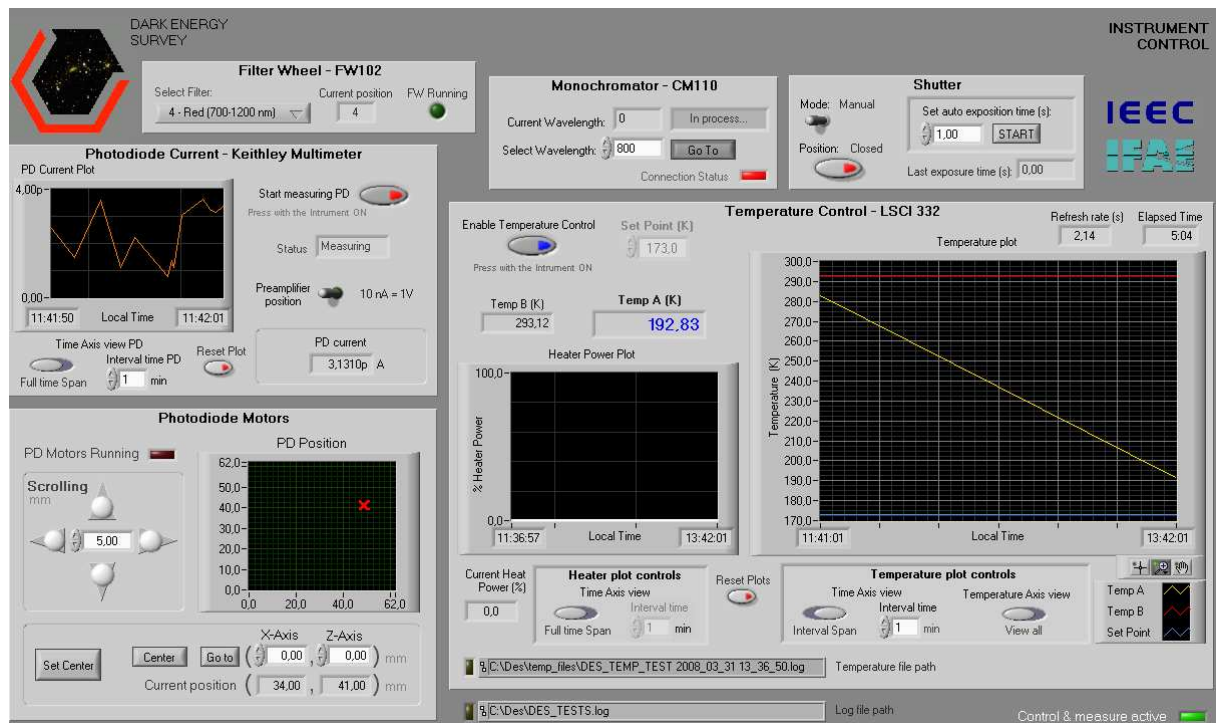


Figure 2.12: The front panel of the controller

Chapter 3

The CCDs and the tests

The Charge Coupled Device (CCD) is a kind of photon detector that converts the incident light into electrical signal. It basically consists of arrays of capacitors sensitive to the light, where electrons are generated by the incident photons through the photoelectric effect, and then captured. The packets of charge are not initially converted to an electrical signal, but are moved in one direction to the successive capacitors by placing the capacitors very close to one another, and manipulating the voltages on the gate of the capacitors to allow the charge to spill from one capacitor to the next. A charge detection amplifier placed at the end of the chain detects the presence of the charge packet, providing an output voltage that can be processed. With this set of signals it is possible to make a map and reproduce an image.

History

In the late 60s, Willard Boyle and George Smith were working in a Bell Labs group interested in creating a new kind of semiconductor memory for computers. On October 17, 1969 they invented a memory device which consisted of a simple row of metal plates where the electrical charge was transferred from one to the next by clock signals. The amount of charge could be saved in one plate and could be read transferring the charges in the opposite way. This was the basic structure and principle of operation of the CCDs.

Although the CCD was originally conceived as a memory device, it became immediately clear that it had potential uses that ranged far wider than simple memory applications. The CCD was used both to store voice in the telephone answering machines, and to delay a discrete time an analog signal in order to synchronize it with another one. But the most important application is for the production of images, which started when astronomers recognized that the CCD could be used for imaging using array areas. This new kind of detectors had a significantly higher sensitivity than the devices of that time: photographic film and vidicon tubes. In 1983, telescopes were first outfitted with CCD cameras. These cameras allowed the near-infrared stars to be detected, because the range in wavelengths the CCDs is able to detect is wider than the optical window. For many reasons the CCD displaced other sensors within a few years, becoming nowadays the most used photon detector.

Background

As mentioned above, a CCD basically consists of arrays of Metal Oxide Semiconductor (MOS) capacitors. These capacitors have the particularity of being made by a semiconductor substrate, an oxide insulator and a metal gate. Usually the silicon is used as the substrate material. The insulator, in the form of a silicon dioxide layer is grown on top of the substrate. The capacitor is finished off by placing an electrode on the top of the insulating silicon dioxide. These electrodes are recently made of a heavily doped polycrystalline silicon conducting layer (polysilicon) instead of any kind of metal. However, the silicon that forms the base and the top layer is special in nature. It is a silicon doped with a small amount of some other material. Doping allows materials to be exploited through different electrical means, due to their different electronic configuration.

A silicon atom has four valence electrons that it can share with adjacent atoms in order to form up to four bonds. In a crystal of pure silicon, all atoms (except on the surface) would be perfectly bonded to four neighboring atoms, without neither extra electrons nor places where electrons are missing. If we introduce into the perfect crystal a doping element with only three electrons available for bonding, this atom will form three normal bonds but it leaves a hole of a neighbour silicon atom without forming any bond. What is interesting here is that this "hole" actually can move around the entire crystal. An electron nearby can move to fill in the original hole, but in eliminating the original hole, it has created a new hole. Effectively, this hole is able to move around just as freely as a mobile electron. Such a material, one that contains extra holes, is called a p-type material. In the case the doping element has five available electrons, it would be called an n-type material. It is important to note that these materials are all neutral and that extra electrons or extra holes in this case do not make the materials charged but merely indicates what kind of charge is able to move inside them.

We can control the motion of these extra electrons or holes by applying different electrical fields or voltages on the gates. In figure 3.1 is represented a global n-type substrate and an oxide layer with several gates. After connecting the substrate to the ground, we apply a negative voltage $-V$ on one gate and leave the next gates without bias. The negative voltage generates an electric field that repels the free electrons of the n-type substrate to the ground separating them from the oxide. In consequence the ions in the substrate next to the oxide rest positive charged, forming a depletion region, where there are not free charge carriers. The depth of

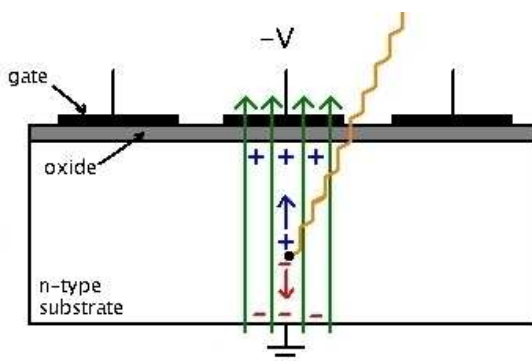


Figure 3.1: A MOS capacitor with surface channel. The charges are accumulated in the interface between the n-type substrate and the oxide.

this region depends on the voltage applied. When a photon with enough energy to pull out an electron from its atomic bond interacts with the silicon of the substrate, a free electron-hole pair is generated. The electron is repelled by the electric field generated by the voltage $-V$ to the ground, while the hole is occupied by a neighbour electron generating a new hole, moving a global hole towards the oxide interface. These holes generated by an incident photon are the charges we can measure, because are not due to the doping of the n-type substrate. If the substrate would be a p-type, the voltage would be positive, and all the processes would happen in the opposite way.

In the case we have been discussing, the charges are accumulated next to the substrate-oxide interface, in what is called *surface channel* MOS capacitors. However it is possible to accumulate charge by another way, through a *buried channel*. In this case the minimum of the potential well, where the channel will form, is entirely within a p-type layer, away from the problems caused by surface irregularities at the interface of the oxide and semiconductor. Although both surface channel and buried channel MOS capacitors have been utilized in CCD construction, most scientific CCDs uses the buried channel. In order to implement the buried channel a thin p-type region is formed between the n-type substrate and the oxide layer, as can be seen in figure 3.2.

When a p-type and an n-type material are brought into contact, a p-n junction is formed and a very interesting result occurs. Extra electrons from the n-type material will diffuse to the p-type material and fill in some of the extra holes from the p-type material. The diffusion and recombination of electron-hole pairs across the boundary directly results in the n-type material becoming positively charged and the p-type material becoming negatively charged. Recall that before the two materials were brought into contact and before diffusion occurred, they were both neutral. As diffusion occurs and the n-type and p-type materials become increasingly charged, an electric field is generated around the contact boundary. This electric field eventually slows and stops the diffusion of charge across the boundary. When diffusion stops, there are no more extra electrons or holes around the boundary; they have all recombined. In this case the depletion region is surrounding the boundary in which electrons and holes have recombined. Outside of the depletion region, extra electrons still remain in the n-type material and extra holes remain in the p-type material.

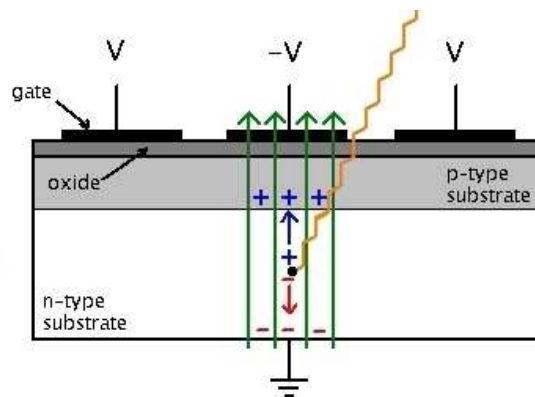


Figure 3.2: A MOS capacitor with a buried channel. The charges are accumulated inside the p-type layer.

Read-out

Once holes are generated in the depletion region and accumulated, we want to measure how many photons have interacted with the substrate. In other words, we want to read the CCD. To do this, the charge packets must be transferred to another device for data processing. This is accomplished by sequentially changing the applied voltage at the gates. The schematic process is shown in figure 3.3. First, we have the holes in a potential well generated by the bias of the central MOS capacitor. The voltages of the neighbour gates are polarized to the opposite voltage of the central capacitor, in order to increase the walls of the potential well. In a n-type substrate, the central capacitor is biased negatively, and the ones of the sides positively. Then we apply the same bias voltage to the closest gate in the direction the processing data goes. This causes the holes to divide between the two wells. Then, the potential of the gate where the holes originally were, is raised over a finite time interval so that the gate now becomes a potential barrier. The gate next to the original populated gate but in the other direction is maintained at constant potential during this entire process to keep the charge packets from moving back. Now, the charge packet has moved over one gate. In a CCD, the capacitors are grouped in threes. This group is called pixel and it will be a point in the final image. The sequential reading is repeated three times to displace the charge one pixel. This cycle is then repeated over and over in fractions of a second to transfer all the charge packets off the CCD. In figure 3.4 we can see the same method that is used in CCD to read the pixels but using buckets to measure the rainfall in a field.

As mentioned above, a CCD consists of various arrays of MOS capacitors. These capacitors are organized in rows and columns. The resolution of the device is measured both according to how many columns and rows are, and the size of the pixel. Every column is insulated from the contiguous in order to only allow the reading process from top to bottom. So, this region is called parallel register. The charge packet of the last capacitor in each column is also transferred to a different array of capacitors system, which can transfer the charge packets horizontally. This system is a single array of MOS capacitors placed outside the rows and columns matrix, and is called serial output register. When a vertical transfer cycle is done (when the charges have been moved one pixel), then the serial register has all charge packets that had previously been in the last row of the CCD, and the packets are also moved using the same sequential change of voltages but horizontally. At the end of the serial register there is a gate, called sense

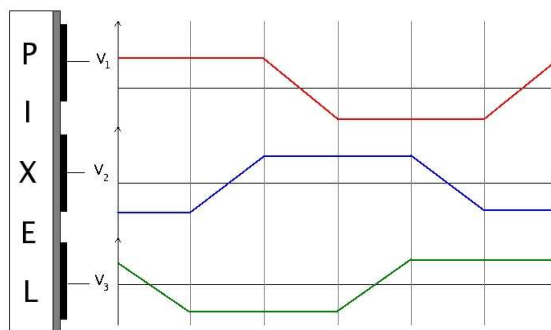


Figure 3.3: Voltages of the three capacitors of one pixel

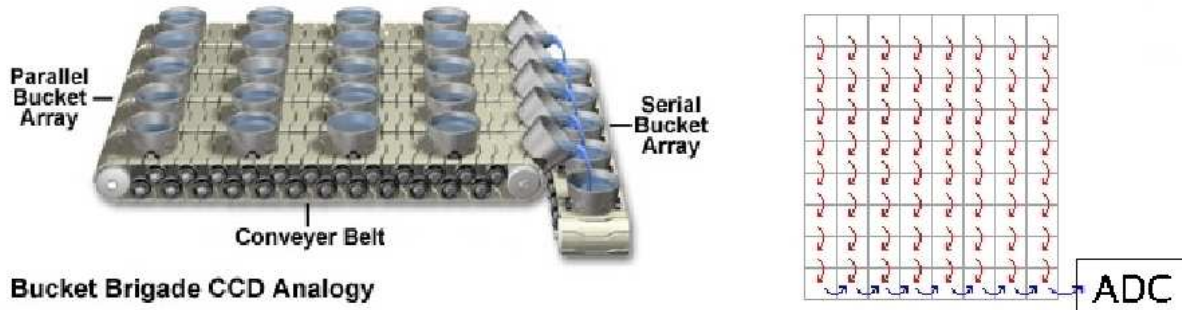


Figure 3.4: The concept of the CCD charge transfer as a bucket system to collect the rainfall at different points in a field. Once the rain has stopped, the buckets in each row are moved down horizontally across the field on conveyor belts. As the buckets in each column reach the end of the conveyor, they are emptied into another bucket system on a vertical belt that carries it to a metering station where its contents are measured.

node, that transfers each packet to an Analogical to Digital Converter (ADC) device, where the charge packet is translated to digital signal and sent to an acquisition card in the electronic readout system. Once the serial register is emptied pixel to pixel into the ADC, a new vertical cycle is done in order to transfer the original penultimate row, now with its charge packets in the last row, to the serial register. A complete serial register readout has to be done before each vertical cycle, because in this way the serial register is emptied and prepared to be filled with another row of charge packets.

The ADC converts the analog signal (packet of holes or electrons) into a digital signal (a voltage). This digital signal is controlled by the readout electronic system, which sends it to a computer where is recorded in a file. At the end of the whole lecture process, this file contains all the measures of the CCD pixels. Plotting them in the correct order, it is possible to reconstruct an image, which represents the electron distribution over the CCD, generated by incoming light.

Illumination

The photons can come from everywhere, but the CCDs are constructed differently depending on where we want the photons to interact. CCDs where the light penetrates through the gate structure to reach the region where electrons are collected, are called front-illuminated. Because of the high absorption coefficient for short wavelength photons in silicon, the capability of collect photons in the blue and ultraviolet regions is poor in front-illuminated CCDs. More sophisticated in the production, but with a higher sensitivity, are CCDs exposed from the opposite side. These CCDs are called back-illuminated. To insure charge transport from the back to the front side where the electrons are collected, the silicon bulk is thinned. Both the front and the back-illuminated CCDs can be constructed with surface or buried channels.

Noise

The picture in a CCD is represented by the electron distribution on the CCD chip. But not all electrons give useful information of the pictured object. Noise manifests itself during two main processes: the collection of electrons and the transfer of charge packets.

During the collection of electrons, the thermal noise is one of the biggest error sources. Over time, electrons can be thermally excited into the conduction band and move freely in the depletion region, masking the stored information. To minimize the effects of thermal noise, CCDs are usually cooled to low temperatures, typically around 160 K. The dark count is the amount of generated electrons by thermal process. Images that include this dark count can be corrected by subtracting a so call dark frame, a picture taken with a closed shutter which contains the count from thermally released electrons. This dark count is highly temperature and exposure time dependent and typically doubles for a temperature change of 5 to 10 Kelvin. Another source of noise can be the called *shot noise*, the fluctuations associated to the quantum efficiency. For two different exposures illuminated by the same light, the number of e-h pairs generated can be different. Apart from these, another source of contamination can be the light from sources other than the desired one (light pollution).

During the charge packet transfer, efficiency is a major concern. Whenever charge is transferred, a small amount is left behind, and this *residue* blurs the image. It cannot be solved but it can be reduced increasing the bias voltages in order to make the walls of the potential wells higher. Charge transfer efficiency must be greater than 99.9% because it increases exponentially with the number of transfers made. A value of 99.9% translates into only 36% of the original charge conserved after 1000 transfers.

3.1 DES CCDs

The DES collaboration has proposed the construction of DECam, a CCD mosaic camera, in order to take the images through which it can achieve its scientific goals. For this purpose it has selected a 250 μm thick, 15 μm pixel size and back-illuminated CCD, designed and developed at the Lawrence Berkeley National Laboratory (LBNL). The thickness of the LBNL design has two important implications for DES: fringing (discussed below) is eliminated, and the quantum efficiency of these devices is more than 50% in the z band (700 nm to 1100 nm).

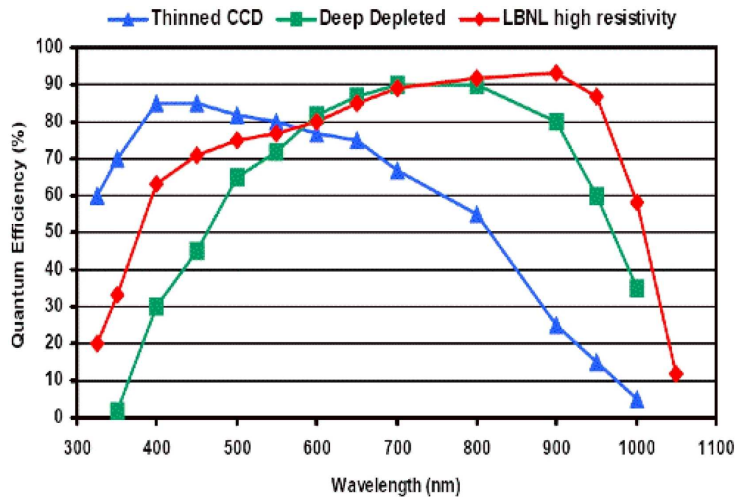


Figure 3.5: The quantum efficiency of different types of CCDs as a function of wavelength. It is obvious that the LBNL high resistivity CCDs are more sensitive at near-infrared wavelengths.

The fringing of CCD detectors occurs because of interference in the depletion region between the incident light and the light internally reflected at the interfaces between the thin layers of the CCD chip. There is a minimal thickness of the substrate to absorb light of a specified wavelength. In a thinned CCD, the thickness is not enough to absorb a photon of more than 850 nm. The $250\ \mu\text{m}$ CCDs are able to absorb light up to more than 1000 nm. On the other hand, the back illumination allows a good blue response because the light falls directly on the substrate without going through the gates and the oxide, where the UV light could be absorbed.

The quantum efficiency (QE), the ratio of incident photons to generated electron-holes pairs, is a good indicator of whether a CCD is able to produce good results for science applications. The standard astronomical CCDs typically have a QE at 1000 nm of 5-10% because the charge collection region is $10\text{-}20\ \mu\text{m}$ thick and the total device thickness is often less than $50\ \mu\text{m}$. The absorption length in silicon is $205\ \mu\text{m}$ at a wavelength of 1000 nm. In this way, the QE of these $250\ \mu\text{m}$ CCDs in the infrared wavelengths is a factor 10 higher than traditional thinned astronomical devices, as it is shown in figure 3.5.

The LBNL CCDs have the conventional three-phase structure: a polysilicon gate, a dielectric layer of SiO_2 , and a high-resistivity n-type substrate. In this case, a p-type silicon layer has been introduced between the dielectric and the substrate in order to produce a buried channel. The choice of n-substrate/p-channel over the more conventional p-substrate/n-channel was due to the fact that it was found more straightforward to transfer holes than electrons [11]. Unlike conventional CCDs, in this case the charge carriers are holes, not electrons. At the backside of the substrate a 3-layer coating has been added. Firstly a 10 nm layer of n-doped polysilicon used as an interface layer, then a layer of Indium Tin oxide (ITO) used as electrode to apply the bias voltage, and finally a 100 nm layer of SiO_2 . These layers are transparent for UV/Visible light and their thickness was chosen to minimize reflection. Figure 3.6 shows a schematic cross section of the LBNL CCD compared with other conventional designs.

The design of the CCD chip is as explained above: a set of arrays of many capacitors

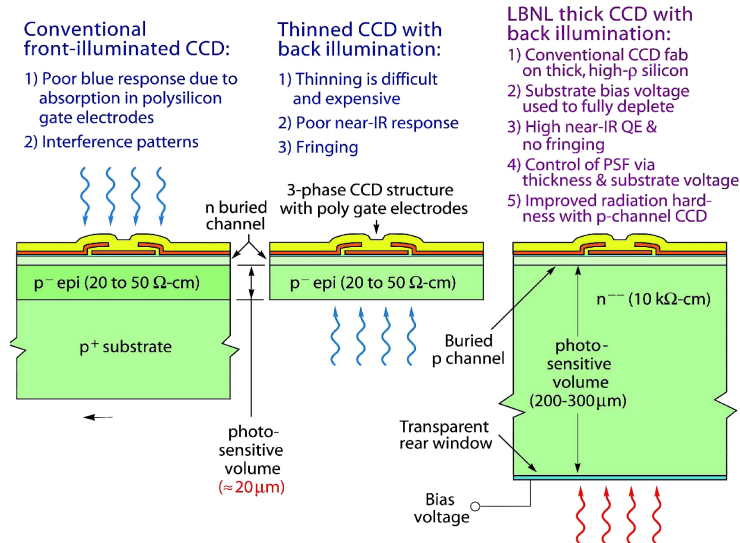


Figure 3.6: Cross sections of three types of CCDs. DES has selected the last one, a $250\ \mu\text{m}$ thick with buried channel and back-illumination.

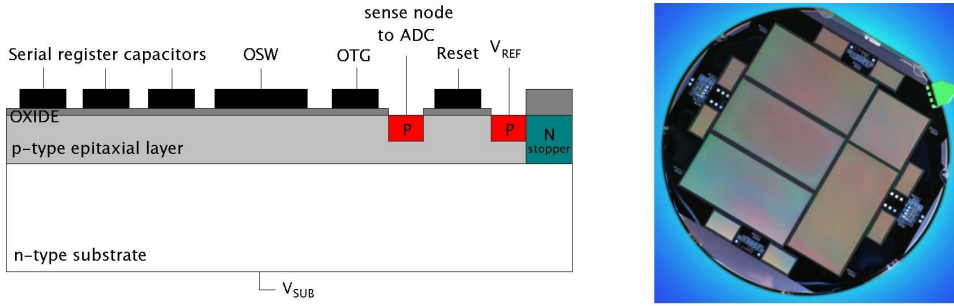


Figure 3.7: Left: Cross section of the last part of the serial register. One can see the last transfer gates, the Output Summing Well (OSW), the Output Transfer Gate (OTG), the sense node, the reset switch and the place where V_{REF} is connected to the CCD. V_{SUB} is applied in order to achieve the full depletion in the device. Right: An LBNL 6 inch diameter silicon wafer where different sized CCDs are placed.

arranged in threes forming pixels. At the end of the vertical arrays there are two independent serial registers able to displace the charges horizontally, the left one (L) for the left half of arrays and the right one (U) for the other half. At the end of each serial register there are extra capacitors before the ADC. The first is called Output Summing Well (OSW) which is a wider gate clocked independently and it is used to perform the pixel-binning, in the case one wants to add various pixels, increasing the sensitivity but cutting the resolution of the final image. Next to the OSW there is the Output Transfer Gate (OTG) which is nonclocked and it is used to reduce the clock feed-through signal generated by the OSW when charge is dumped onto the sense node. Both OSW and OTG can also be used to inject electrical charge into the horizontal serial register when the CCD is used as a storage device. Next to the OTG there is a space filled with a p-type silicon piece, which is called sense node. Here is where the charge packet is converted into a voltage, because it is connected to the ADC. The last capacitor of the serial register is the reset switch, which is responsible for resetting the sense node to a reference voltage (V_{REF}) before charge is transferred from OTG into the sense node. Just before the end of the register and next to the reset switch there is another p-type silicon piece where the bias voltage V_{REF} is introduced. In figure 3.7 it is shown a scheme of the last part of the right horizontal serial register where all these gates and connections can be seen.

These CCDs are not produced one at a time because it wouldn't be economical or efficient. LBNL produces a 6 inch diameter silicon wafers where different sizes of rectangular CCD are placed. In each wafer they fit four $4k \times 2k$ pixel CCD, one $2k \times 2k$ pixel CCD, and eight 1024×512 pixel CCD. The most important are the biggest because sixty-two of them will be placed at the focal plane in the DECam, together with twelve $2k \times 2k$ placed at the edges of the focal plane and used four for guiding, four for focusing and four for alignment purposes. The little ones are not necessary but are produced to make the most of the wafer and are only used for testing. A complete LBNL wafer with its different CCD chips, is shown in figure 3.7.

In the SLAB we have a set of these LBNL CCDs. As the $4K \times 2K$ CCDs are tested in FNAL, we have been doing our tests with the little $1K \times 0.5K$ ones. We have two front-illuminated CCDs all with p-type buried channel, two double front-illuminated which can produce side-by-side images, and three back-illuminated with the same kind of channel. Figure 3.8 shows two of them, a double front-illuminated and a back CCD.

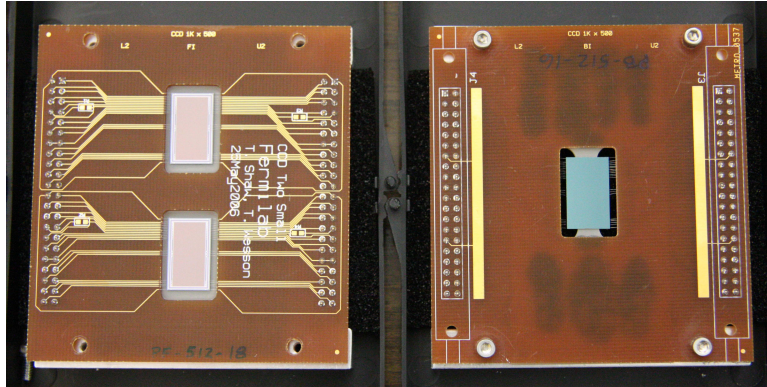


Figure 3.8: A double front-illuminated DES CCD (PF-512-18) for test on the left, and a 1024×512 pixel back-illuminated CCD (PB-512-16) on the right.

3.2 The tests

In this section the set of tests which are carried out in the SLAB is explained. Similar tests are already done at LBNL before sending the CCDs together with a table with all the operational voltage values of the different gates of the chips. Nevertheless we use these tests in order both to check these values and because DES has increased the requirements that a CCD has to fulfil. The different tests can be arranged according to the tasks a CCD can perform in generating an image:

- *Charge generation:* the ability to intercept an incoming photon and generate an electric charge through the photoelectric effect. The quantum efficiency, the ratio of incident photons to generated electron-hole pairs, is the parameter that tells us how well the CCD accomplishes this task, which is heavily dependent on the energy of the incident photon. Photoelectric effect interaction only occurs if the photon has enough energy to excite an electron into the conduction band (~ 1.14 eV for silicon), if not it passes through the chip. Photons with energies up to 3.1 eV only generate a single electron-hole pair, while energies greater than 3.1 eV produce multiple e-h pairs. Photon energy can be converted to a wavelength by:

$$\lambda = \frac{hc}{E} = \frac{4.135 \times 10^{-15} eV \cdot s}{E(eV)} \frac{3 \times 10^8 \frac{m}{s}}{s} = \frac{1240.5 \text{ eV nm}}{E(eV)} \quad (3.1)$$

from this equation can be seen that UV photons begin to generate more than one e-h pair. An ideal CCD would intercept incoming photons of all wavelengths, however there are some ways that make the QE decrease. In front-illuminated CCDs, the photons must pass through the gates before they interact with the substrate. Gate absorption is an important way to lose QE, for this reason the back illumination improves the charge generation. Reflection is another QE loss problem, but can be reduced by depositing antireflection coatings on the surface. Then, the most significance reason for which QE is reduced is the transmission loss. It takes place when incoming photons pass through the CCD photosensitive volume without generating signal charge. This problem is pronounced above the near-infrared (above 700 nm) and soft x-ray (below 0.2 nm) spectral regions.

- *Charge collection:* the ability to accurately reproduce an image from the electrons generated. It has to take into account three parameters: the amount of pixels the CCD has, the charge a single pixel can hold (also called the well capacity), and the pixel efficiency to collect the electrons generated. In the first two, the bigger is the better. The more pixels a CCD has, the more resolution the final image has; and the greater the full-well capacity is, the greater the dynamic range (relation between brightest and faintest objects) and the signal-to-noise relation are. On the other hand, the efficiency in collecting the generated electrons is the most critical parameter and it is related to the diffusion of charge among pixels. This task drives us to measure how well a CCD can record and reproduce the spatial information.
- *Charge transfer:* the ability to transfer collected charge from one potential well to the next one. To accomplish this task one has to manipulate efficiently the clock voltages on the parallel and serial registers in order to lose as little charge as possible during the transfer process. Since the full-well capacity could be ~ 200000 electrons, a 99% of efficiency wouldn't be a good result because after transfer this charge through 100 pixels, only 73000 electrons would arrive at the last one. Current limits achieve efficiencies of 99.99999%, which is equivalent to a loss of only two electrons in the previous example.
- *Charge measurement:* the ability to detect and measure the charge collected in each pixel. A good measurement is achieved when the charge that arrives at the sense node is well transformed into a voltage proportional to the signal charge transferred. The parameter related with this task is the amplifier's gain. Due to the relation between the capacity and the voltage ($Q=CV$), the tinier the capacity of the sense node is, the higher the amplifier's gain and the greater the output signal. Another problem to take into account is the noise generated by the read-out amplifier, because it is an active element and needs an external source of power. This noise is due to the random fluctuations of the current that flows through the transistor. The previous tasks are noiseless, and the thermal noise can be eliminated by cooling the detector. This makes the amplifier noise the worst problem for a correct measurement. Nowadays, high-performance CCDs have slightly less than $1 e^-$ of noise.

A summary of the parameters measured in the tests and the CCD performance function which they are related to is shown in table 3.1. It is important to remark both that we can measure more than one parameter in one test, and that one parameter can be measured through more than one test. This allows us to compare results for the same parameter obtained differently. The table 3.2 shows the operation voltages LBNL has given with the CCDs. These are the voltages LBNL tells us we have to supply to the CCD to pass the DES requirements. We initially check that the CCD works correctly and then we will change them to try to improve the CCD response.

After some attempts, finally we decided to carry out the tests with the monochromator always on the position that only the 800 nm light can pass through it, because at this wavelength the QE of the LBNL CCDs is higher. In order to reduce the thermal noise we also have decreased the temperature inside the DES cube to 173 K and the pressure to 10^{-6} mbar .

When all the images of tests are taken with *MecStart* and stored in the Slab computer, an automatic script analyzes them and produces a pdf file. In its first page a table with the value of all the parameters is shown, and then all the plots of the tests, described below, are plotted.

Table 3.1: Relation between the parameters measured in a test, the test in which the parameter is measured, and the corresponding CCD task.

Parameter	Test	Task
Dark count	PTC	Charge generation
Linearity	PTC	Charge measurement
Full-well capacity	PTC	Charge collection
Amplifier's gain	PTC	Charge measurement
Pedestal	PTC	Charge collection
Amplifier's gain	MUON	Charge measurement
Diffusion	MUON	Charge collection
Charge transfer efficiency	MUON	Charge transfer
Energy Vs ADU	MUON	Charge measurement
Amplifier's noise	NOISE	Charge measurement
Charge transfer efficiency	CTI	Charge transfer
Charge transfer efficiency	XRAY	Charge transfer
Energy Vs ADU	XRAY	Charge measurement

Table 3.2: LBNL CCD operational voltages.

Signal	Typical voltage (V)
Substrate bias (V_{SUB})	40
Reset drain (V_{REF})	-12
Output transfer gate (V_{OTG})	3.5
Vertical clocks (V_1, V_2, V_3)	5.5, -2.5, 5.5
Horizontal clocks (H_1, H_2, H_3)	8.5, -3.5, 8.5
Output Summing well (V_{OSW})	-4

The goal of the test, the procedure, the kind of images needed (dark, illuminated, clear...), and the number of images taken, have been explained in each test. The regions of the images that the analysis code uses for each test, as well as the procedures for computing values and errors, are explicitly detailed in appendix A.

3.2.1 Output transfer gate test (*OTG*)

The first test is called OTG, and it will show us many useful things to take into account before start making any other test, such as the effective threshold voltage (V_{EFF}), and the polarization at which the charge injection into the CCD occurs, in order to know whether the CCD is working as a memory or detector device.

As it is explained in the previous section, a buried-channel CCD can be thought as a p-n (n-substrate and p-epitaxial layer) junction with an insulator and a gate at the exterior of the p-side surface. A depletion region appears around the p-n junction, and its width can be increased up to achieve a full depletion of the substrate. This is performed by supplying a

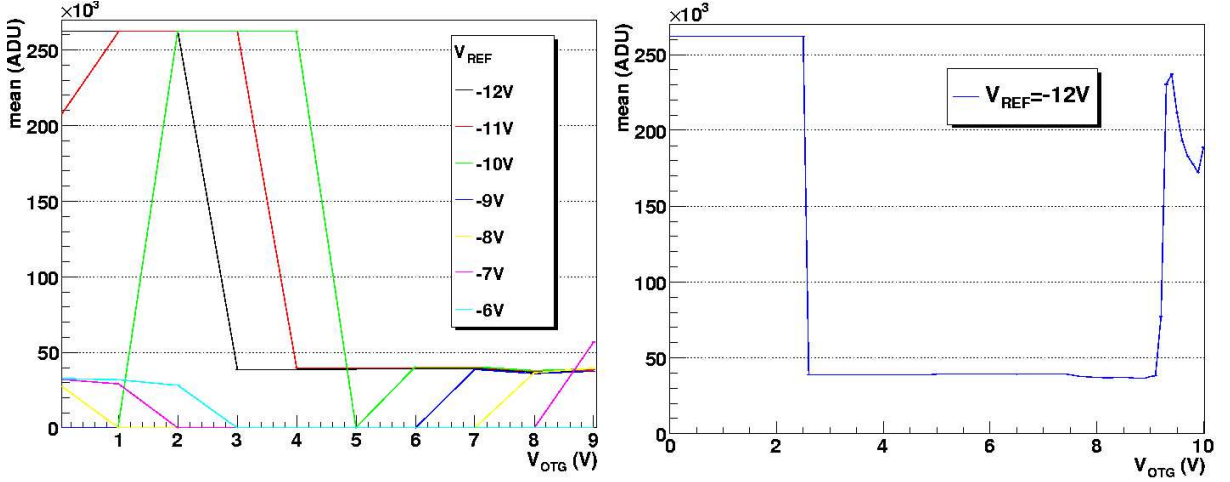


Figure 3.9: The charge injection effect is shown in these plots, where the mean counts are plotted as a function of V_{OTG} , for different values of V_{REF} . The OTG test on the left, and the VOTGSCAN on the right. In VOTGSCAN, V_{REF} is fixed at -12 V because this is the operational voltage given by LBNL.

positive voltage V_{SUB} through the bottom side of the substrate. Then, when applying a gate voltage (V_G), the holes in the p-layer will be repelled away from the surface, thereby creating a new surface depletion region. The buried channel is the region between the two depletion regions. Decreasing V_G for a fixed V_{REF} voltage, makes deeper the potential well. Increasing V_{REF} for a fixed V_G , makes wider the surface depletion region. The reference voltage at which the two depletion regions meet in the buried channel is called V_{MAX} meaning that the maximum channel potential is found. This value depends on both the gate voltage and on V_{REF} .

Then, the effective threshold voltage V_{EFF} can be defined as the difference between the gate voltage applied and V_{MAX} .

$$V_{EFF} = V_{MAX} - V_G \quad (3.2)$$

This equation is used to make clock adjustments and achieve optimum performance. The effective threshold is one of the most important parameters that is measured when characterizing CCDs, because it is a critical process parameter for the CCD manufacturer. One can know a lot about it through the effective threshold value.

On the other hand, it would be interesting to know how a CCD can be used as a memory device. Charge injection occurs when the gate voltage applied at the output transfer gate (V_{OTG}) and at the output summing well (V_{OSW}) are biased together negative relative to V_{REF} . Under this condition, charge from the output diode is injected under the OTG and the OSW. Then this charge can be clocked in the opposite way than in the read-out procedure, moving it to the horizontal serial register and then to the vertical arrays. Anyway, today charge injection is rarely used in CCD imaging applications.

The OTG test is used to measure the effective threshold voltage (V_{EFF}), from the difference between the reference voltage and the output transfer gate voltage at which the charge injection occurs ($V_{OTG/CI}$).

$$V_{EFF} = V_{REF} - V_{OTG/CI} \quad (3.3)$$

For this, we take a set of 140 images changing the value of V_{OTG} (from 0 to 9 V) for a fixed

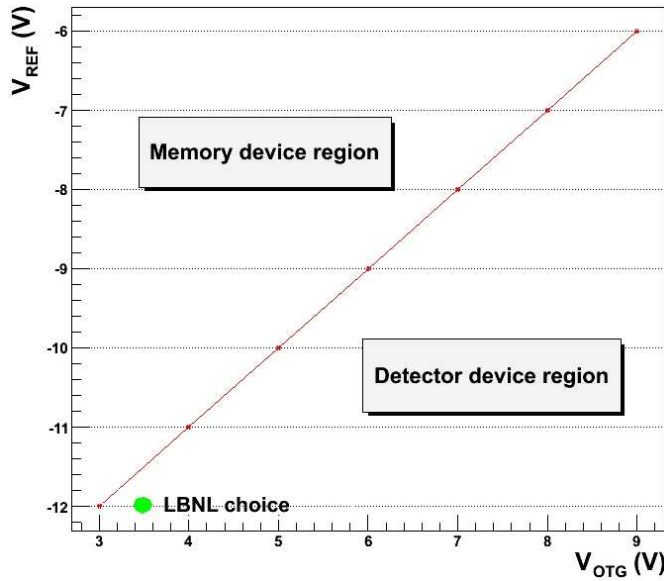


Figure 3.10: V_{REF} as a function of $V_{OTG/CI}$, the value of the voltage V_{OTG} when the charge injection occurs. It can be seen the constant behavior of V_{EFF} , which for this CCD is -15 V.

value of V_{REF} (ranging from -12 to -6 V). For each pair of values we take first a clear image (a read-out used to empty the potential wells) and then a new image of 20 seconds of light exposure.

It is usual and interesting that an image has more pixels than the CCD has. This can be purposely done by overclocking the serial register generating an extended pixel region in the image, also called overscan region. This region is useful to measure the zero charge because is not affected by dark current or other sources of charge.

From the light exposed image, two areas of the overscan region are selected, one for each amplifier (U and L), and the mean digital count (ADU) is plotted as a function of V_{OTG} . Figure 3.9 shows these curves for each value of V_{REF} , at the right (U) amplifier. We can also see for which values of V_{REF} and V_{OTG} the CCD is working as a memory device or as a detector. As we want to use it as a imaging detector we want to work in the flat region. LBNL give us a reference guide where V_{REF} voltage has to be -12 V, and V_{OTG} 3.5 V. This point is indeed in that region.

In order to check this more precisely we have also done another test (VOTGSCAN) increasing V_{OTG} by 0.1 V steps, only for the operating voltage $V_{REF} = -12$ V. This allows us to reduce the error of the voltage at which the charge injection occurs. In this plot we are able to see at which voltage the charge injection occurs, and then plot V_{REF} as a function of $V_{OTG/CI}$. The result is shown in figure 3.10, where it can be seen that V_{EFF} is constant.

We must comment on the valleys of the curves in figure 3.9 for $V_{REF} > -10$ V. This occurs for the pair of values V_{REF} and V_{OTG} at which the two depletion regions meet and there is no channel between them.

3.2.2 Photon transfer curve test (PTC)

The photon transfer curve test can be used to evaluate many CCD parameters, but we will only measure a few of them: the full potential well capacity, the linearity of the charge generation with time, the electronic and thermal dark current, the pedestal, and the gain constant, a relation between the electrons measured and the digital counts generated.

The counts of a pixel in the final image is a result of many processes, from the photon that interacts with the chip, to the digital signal the ADC sends to the electronic readout. This digital signal is given by

$$S(ADU) = PQ_E S_V A_V \quad (3.4)$$

where P is the number of incident photons; Q_E is the quantum efficiency, the ratio of incident photons to generated electron-hole pairs; S_V is the sensitivity of the sense node, the Volts per electron it sends to the ADC; and A_V the gain of the ADC and the amplifiers before the ADC.

The PTC test can help us to find a direct relation between the ADUs registered and the electrons in the potential well. We can define,

$$K = \frac{1}{S_V A_V} \quad (3.5)$$

as the camera gain constant, because all these transfer functions depend on the constant voltages applied. The camera gain constant gives us the number of electrons needed to count one digital signal (ADU). Then the signal can be written as,

$$S(ADU) = \frac{PQ_E}{K} \quad (3.6)$$

The K constant can now be determined by relating S to its variance σ_S^2 , using the propagation of errors,

$$\sigma_S^2 = \left[\frac{\partial S}{\partial (PQ_E)} \right]^2 \sigma_{PQ_E}^2 + \left[\frac{\partial S}{\partial (K)} \right]^2 \sigma_K^2 \quad (3.7)$$

Assuming that K has a negligible variance ($\sigma_K^2 = 0$), and $\sigma_{PQ_E}^2 = PQ_E$ from Poisson statistics,

$$K = \frac{S}{\sigma_S^2} \quad (3.8)$$

where K is the camera gain constant when we take S to be the mean observed signal.

In order to measure this camera gain constant and the rest of parameters through the PTC test, we set the operational voltages to the default LBNL values. The PTC test consists of 320 images, eight for each exposure time (T_{exp}) from 1 to 40 seconds. We take twice this group of shots: first a clear image, then we wait the exposure time without opening the shutter and take another image (NOTEXP), after that another clear image, and finally we open the shutter for the exposure time and take the light exposed image (EXP). The clear images are read-outs only used to empty the potential wells, and are not used anymore. From the remaining set of images, the analysis code erases the overscan regions selecting the exposed region. At this time we have all the information needed to evaluate the CCD parameters.

The pairs of exposed images (EXP) at a given T_{exp} are subtracted pixel to pixel to obtain the variance σ_S^2 , and averaged for the calculation of the mean signal S . The procedure is detailed in appendix A. In figure 3.11 the plot of the variance as a function of the mean is shown in red.

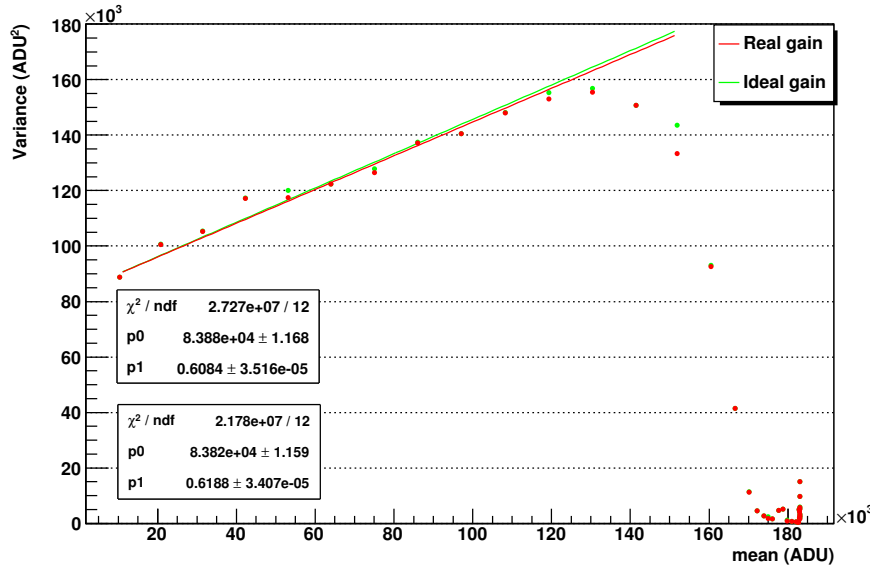


Figure 3.11: Variance as a function of mean obtained by taking a series of paired images with varying exposure time. The mean is measured averaging the two images. The variance subtracting them. The red points measure the real gain, and the green ones the ideal gain, where it is supposed that the mean value of the subtraction is zero. The inverse of the slope of the red fit corresponds to the real camera gain constant (K). In this case $K = 1.64 \pm 0.01 \text{ e}^-/\text{ADU}$. The full-well potential is achieved at about 180000 ADU.

For each exposure time, the variance and the mean increase linearly, until the saturation of the well is reached. Then the mean doesn't depend on T_{exp} because it falls to a constant value. This value is the full potential well. The full well is known as the maximum charge level that the pixel can hold and transfer, and the DES requirement for that value is that must be greater than 130000 e^- . The fit shows the inverse of the parameter K , the value of the slope is the relation ADU/e^- of the CCD. In the figure we also show some points on green corresponding to the assumption that the subtraction of the two exposed images is exactly zero. Because of this, we call it *ideal gain*. It can be seen that the two slopes are very similar, showing that the subtraction is very close to zero.

As mentioned above, more parameters can be measured with these images. We can plot the mean signal S as a function of the exposure time to check the linearity in the response of the device. This is shown on the figure 3.12. In the top plot we can see three set of measurements: the green points are made by averaging the two exposed images (EXP) for each exposure time, the blue points are the average of the two images with the shutter closed (NOTEXP), and finally the red one is the difference between them. These last points are the same used before in the measurement of the camera gain, because they do not have the contribution of the dark current measured with the NOTEXP average. The fits show the increment in ADUs for every exposure time. The green line, also shows the value of the pedestal, which is the point where the fit intercepts the y-axis. The pedestal is the signal generated by the amplifier system and it is taken as a threshold signal.

When the potential well is going to saturate, the points begin to separate from the linear

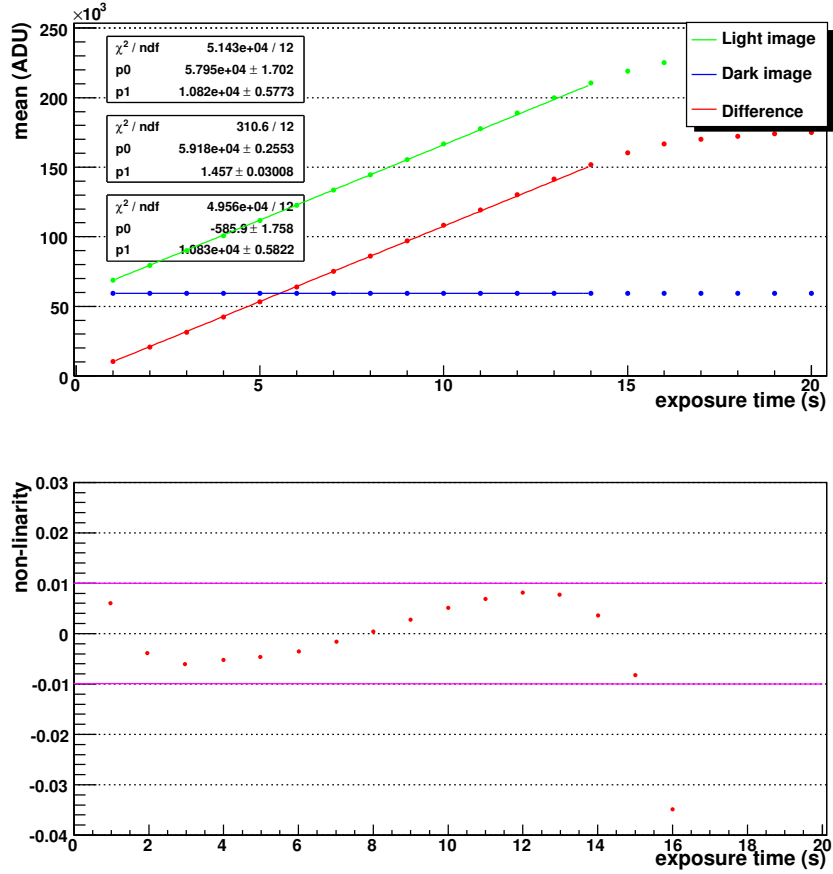


Figure 3.12: The mean as a function of the exposure time is presented on the top. Linear fits are performed in order to see when the linearity is lost. The green one is made by averaging the two exposed images (EXP), the blue points are the average of the two images with the shutter closed (NOTEXP), and finally the red one is the difference between them. Non-linearity defined as the fractional difference between the red points in the top panel and the red fit is plotted on the bottom. The requirement for the non-linearity is to stay below 1%. This CCD does not meet the requirements at about 15 sec.

growth. The DES specification for maximum non-linearity is 1%. The non-linearity can be defined as the difference between the points and the fit. On the bottom in figure 3.11, we show the non-linearity as a function of the exposure time. From the graph, we can clearly see the exposure time at which a CCD does not meet the linearity requirements, about 15 sec.

3.2.3 Muons test (*MUON*)

The muon test is a different way of measuring the camera gain constant K using an image of a cosmic ray. Cosmic rays reaching Earth's surface are predominantly muons. Therefore, it should be possible to compare the expected ionization charge released by muons in silicon with the number of counts observed in the pixels the muon has crossed after subtracting the counts of the dark pixels (pedestal).

For minimum-ionizing particles (mip), such as the muon, the most probable charge deposition

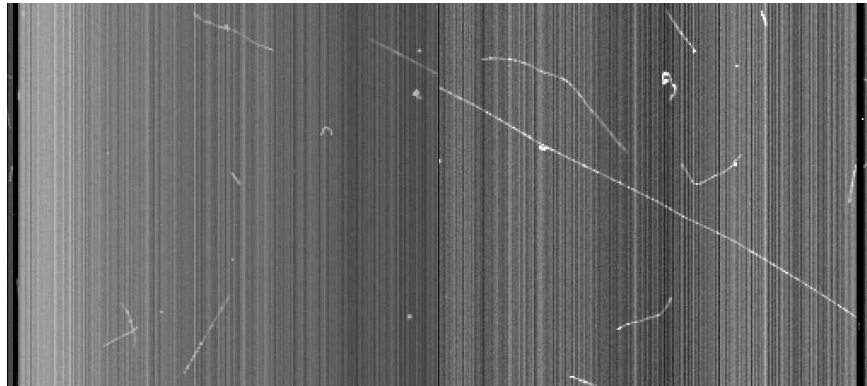


Figure 3.13: A muon image taken at The SLAB. The incident angle is 29.3° , meaning that the muon has passed through a $17.2 \mu\text{m}$ leaving about $1260 e^-$. The difference in counts between the pixels the muon has passed through and those it has not, is 1408. Then the camera gain constant is $1.2 e^-/\text{ADU}$. In the image, smaller muon traces can also be seen.

in a $300 \mu\text{m}$ thick silicon detector is about $22000 e^-$ [15]. This is so because in silicon the most probable ionization energy loss by a particle in the mip regime is about $270 \text{ eV}/\mu\text{m}$ and the energy needed to create an electron-hole pair by ionization is about 3.65 eV . It is important to stress that is not the mean value but the most probable one, because the energy deposition curve is actually a Landau distribution with a long tail and not a Gaussian. For instance, in $160 \mu\text{m}$ of silicon the most probable value for the deposited energy or charge is about 70% of the corresponding mean values, whereas for $80 \mu\text{m}$ is about 60%.

As we have squared pixels of $15 \mu\text{m}$ -side, we should find about 1100 more e^- in the pixels the muon has interacted with than in the pedestal pixels. Taking into account the impact angle, this value can be a little bit larger, up to $1555 e^-$ when the incident muon interacts with an angle of 45° respect to the vertical going through $21.21 \mu\text{m}$ of silicon in each pixel. The difference in the number of counts between a pixel where the muon has passed and another one where it has not (dark), will give us the number of counts equivalent to the electrons generated by the muon. We find ourselves facing a small problem, because the muon could have passed by more than one pixel in the same column, dividing the charge that it leaves in them. Due to the geometry of the CCD and to the impact angle, the muon can only pass through two pixels of the same column. Then we will have to integrate these scattered charges. The images needed to carry out this test are a clear one and a not exposed to light one. We must tune the time we have to wait before the second lecture, because it has to be enough for a muon to interact. Then we subtract the non-exposed image from the clear image, pixel to pixel, in order to remove the pattern the electronics produce in every image. The result is called *clean* image. We can map this clean image in order to see the diffusion of the CCD due both to the depth of the potential well and the transfer voltage values. If the diffusion is pronounced, we should change these voltages. Then we can integrate per columns the charge spread in the wells, in order to take the mean value of counts per pixel the muon generates. Taking this value and the calculated value of electrons generated per pixel, we can find the ratio between them, that is the camera gain constant K . In figure 3.13 there is an image of a muon detected at The Slab, with a gain K of $1.2 e^-/\text{ADU}$.

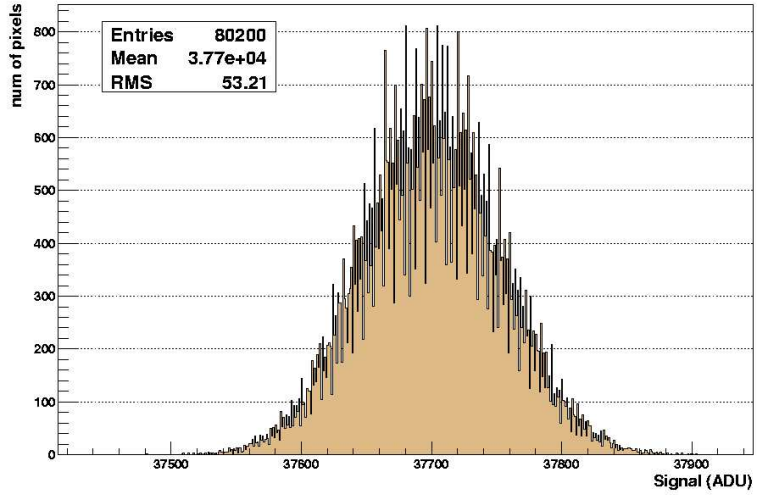


Figure 3.14: All the pixel counts in the overscan region of one image plotted in a histogram. The root mean square of the distribution gives us the value of the noise level. In this case is $\sim 53 e^-/\text{pixel}$, well above DES requirement of $15 e^-/\text{pixel}$. This CCD would not pass the test.

3.2.4 Noise test (*NOISE*)

The NOISE test is a simple measure of the signal measured not coming from interaction with photons. As it is very difficult to disentangle the noise of the external read-out device (electronic noise), from the thermal noise and the shot noise, we consider the measure of the whole chain. The DES requirement is for the noise to be below $15 e^-$ per pixel. This measurement is obtained by computing the spatial root mean square (rms) of the signal in the overscan region, separately for each output channel. This quantity is measured taking ten consecutive lectures, measuring the noise of each one, and averaging their noise value. In the figure 3.14 it can be seen the signal distribution of the overscan region of one of those images, for a CCD with a noise of about $53 e^-$.

3.2.5 Charge transfer inefficiency test (*CTI*)

The next test is the CTI test, a measure of the ability of the device to transfer charge from one potential well to the next. Charge transfer efficiency (CTE) is defined as the ratio of charge transferred from one pixel to the charge initially collected in this pixel. The lost charge from transfers is blurred into the pixels, making the image less clear. We can easily define the charge transfer inefficiency (CTI)

$$CTI = 1 - CTE \quad (3.9)$$

as the fraction of charge left behind a single pixel transfer. DES requirements specify that the CTI has to be less than 10^{-5} . The CTI test is used to study the voltage of the transfer clocks needed in order to get this high efficiency. There are four different voltages to tune: two for the vertical and two for the horizontal clocks. These voltages are those applied to the gates in order to create wells and barriers, thus one is positive and the other is negative.

For this measurement we use the Extended Pixel Edge Response (EPER) technique, where CTE is estimated by measuring the charge deferred by the last exposed pixels in the overscan

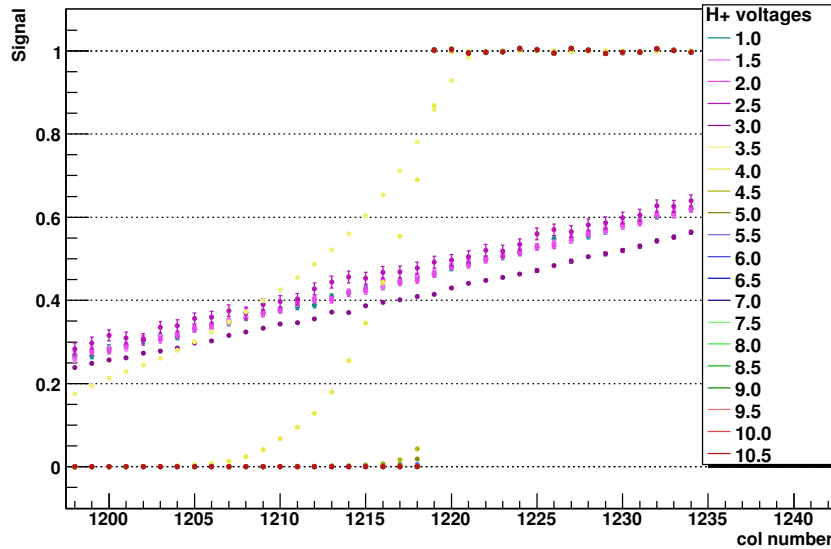


Figure 3.15: The mean of the signal for columns in the transition zone between the exposed and overscan areas, corrected to the mean and the pedestal. The transition between the two regions should be perfectly sharp, although for DES a ratio of 10^{-5} is enough. The different colors represent different values of horizontal clock voltage.

region. We perform a set of ten-second images overclocking the serial register, generating an horizontal extended pixel region, and when the image is completely read-out, we keep generating transfers in order to obtain a vertical overscan region. For each image, we change the value of one of the voltages, maintaining the others on the operational values given by LBNL. A total of 160 images are taken, 40 per voltage. These 40 images are pairs of a clear image and an exposed image, varying the voltage scanned by 0.5 V, the positive ones from 1 to 10.5 V, and the negatives, from -10 to 0 V.

In the case of the horizontal voltages, the transition between the exposed area and the horizontal overscan region is studied. The average of the signal of each column is computed. Then the pedestal is subtracted and the exposed columns are normalized to the mean signal of the exposed area. The final value for each column (S_i)

$$S_i = \frac{\mu_{\text{column } i} - \mu_{\text{pedestal}}}{\mu_{\text{exposed area}} - \mu_{\text{pedestal}}} \quad (3.10)$$

is plotted as a function of the column number.

If the transfer is perfect, the first column of the overscan region must have the same signal as the other columns in the overscan region, and the plot should show a sharp transition. But this does not really happen, because an amount of deferred charge is found in the first extended area columns.

Then the CTI is measured by dividing the averaged signal in the first column in the overscan, by the number of transfers done. In our case, each amplifier reads 256 pixels before the first

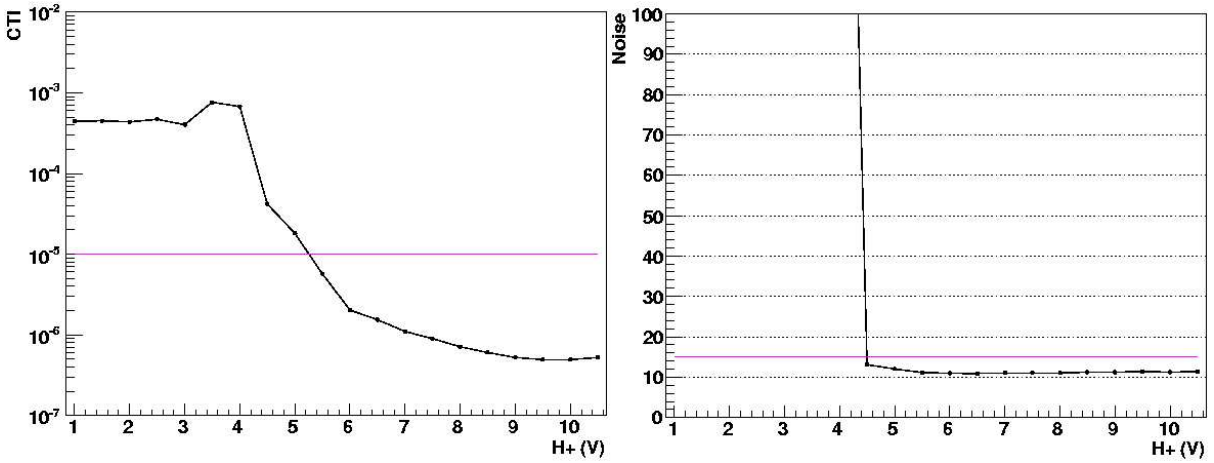


Figure 3.16: On the left, the charge transfer inefficiency as a function of the horizontal clock voltage applied. At voltages above 5 V the DES requirement is satisfied. On the right we plot the noise for each value of the horizontal clock voltage. For small values of the voltage, the transition is not carried out correctly and the noise takes huge values.

pixel of the overscan region. Then

$$CTI = \frac{S_{\text{first overscan column}}}{256} \quad (3.11)$$

In figure 3.15 we show S_i for different values of the positive horizontal voltage, which is scanned from 1 to 10.5 V. For the vertical test, the vertical overscan region is studied, and the same analysis can be done only changing the number of transfers done before the lecture of the first overscan row, which is 1024.

We plot now the measured CTIs as a function of the voltage scanned, in left plot of figure 3.16. We can see that for a voltage above 5 V the DES requirement is achieved. The NOISE test is also performed for every image in order to know how it changes as a function of the voltage value.

3.2.6 X-ray test (*XRAY*)

The XRAY test is performed as an alternative way of measuring both the camera gain constant and the charge transfer inefficiency. The two measurements are done by putting an X-ray source inside the DES cube, at 2 cm from the CCD surface. This is possible because the cube has a knob accessible from the front face which, when turned, presents the X-ray source to the front of the CCD.

An X-ray photon generates multiple e-h pairs in the substrate. In contrast to the visible or near-infrared photons, the electrons are generated in a very small diameter cloud, essentially a near-perfect point source. Then, ideally, the charge generated by an X-ray photon would be collected in a single pixel, but in practice the charge generated diffuses into neighboring pixels.

We have used an ^{241}Am X-ray source to take this measurements. This part of the test consists on taking 100 20 sec images, and plot the signal of every pixel in a signal pixel distribution histogram. The plot should show something like the spectrum of the X-ray source. As we can

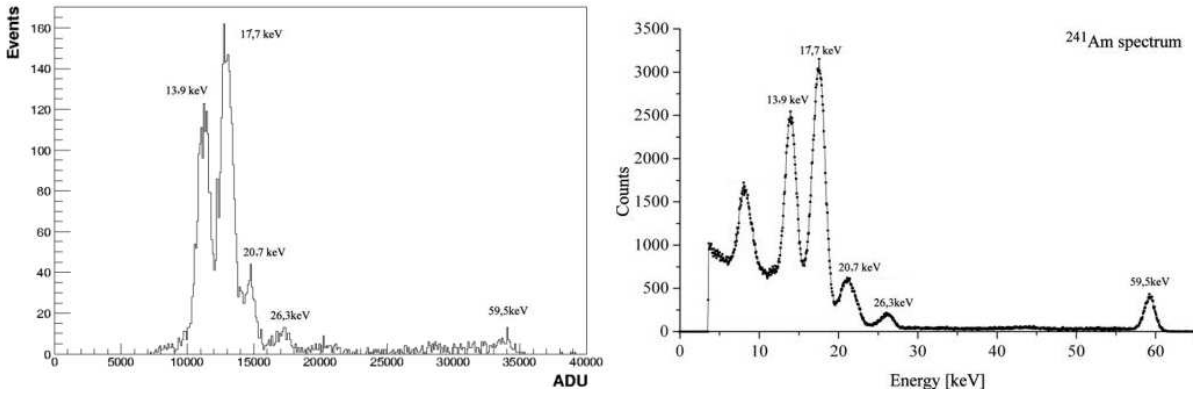


Figure 3.17: Left: Charge distribution obtained from a 20 sec exposure to an ^{241}Am X-ray source. The peak at 8 keV can not be measured because the signal falls in the pedestal region, which is not plotted. Right: An ^{241}Am spectrum, which the measured peaks can be compared with.

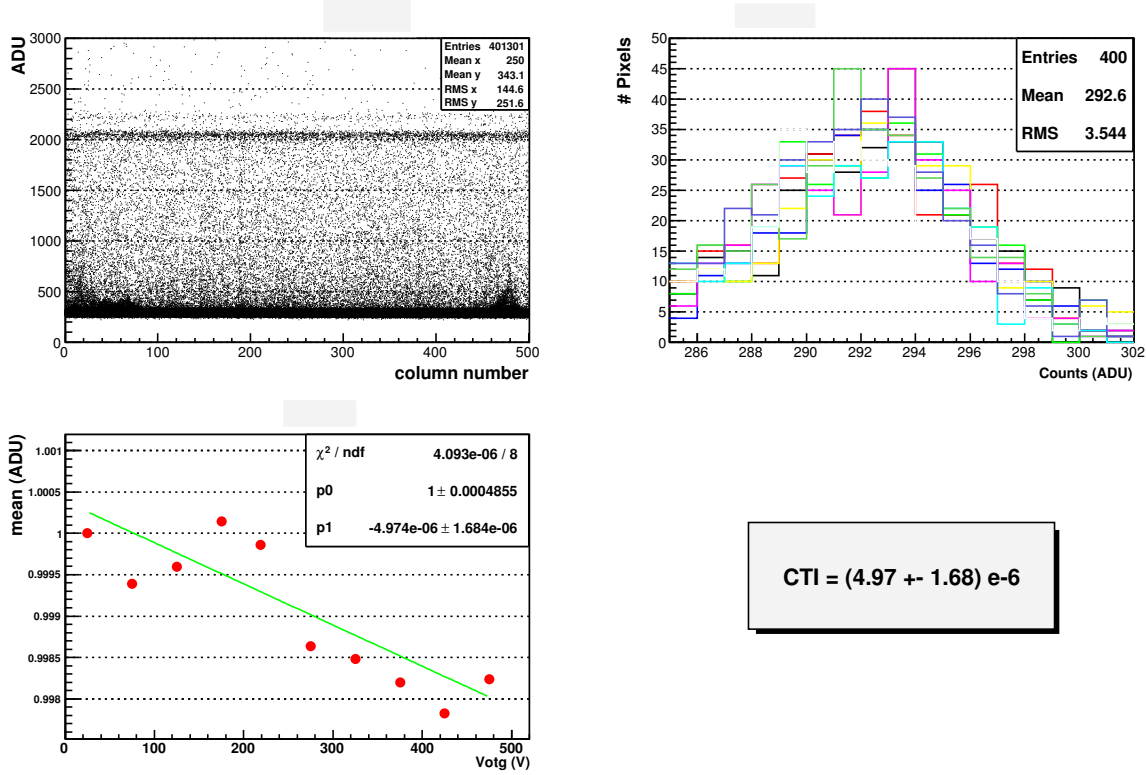


Figure 3.18: Measurement of the charge transfer inefficiency with a ^{55}Fe X-ray source. The distribution of the signal is plotted on the top left panel. Then, in colors, the distribution of signal of the K_{α} peak is done for each fifty columns, and plotted on the top right panel. The mean value of each distribution is plotted and fitted to obtain the CTI value.

compare our distribution to the real spectrum (figure 3.17), we can determine the number of mean counts corresponding to each peak of the spectrum, after the subtraction of the pedestal.

The camera gain constant is derived from the measurement of this subtracted mean signal of the peaks. As the energy required to generate an electron-hole pair by ionization in silicon is $3.6 \text{ eV}/e^-$, dividing the known energy of each peak by the required energy to generate an e-h pair in silicon, we can find the number of pairs generated for each energy. Finally taking the mean signal of the peak we can relate it to the corresponding pairs generated and find the camera gain constant.

For our Americium source, the two peaks that are commonly used are the 13.9 keV one, that generates 3805 e-h pairs, and the 17.7 keV one, that generates 4848 e-h pairs.

The charge transfer efficiency can also be measured with the X-ray technique. This is an absolute measurement because as the number of electrons of the source peaks are known, it is possible to compute the numbers of electrons left in the transfers.

In this case a ^{55}Fe source is used. In figure 3.18 we show a histogram containing the signal counts of all the pixels of a 20 seconds exposed X-ray image, plotted by columns. A more dense cloud at the bottom corresponds to the pedestal signal, the central blurred cloud contains the split or partial events, and the little dense lines are the source peaks. The peak K_α (5.9 keV) can easily be seen as a horizontal dense little cloud in the plot. But it is not really horizontal, it slightly decreases as a consequence of the inefficiency of the transfer process. The measurement of this slope is the value of the CTI. In order to measure it, the mean value of the K_α peak is obtained in every fifty columns. Fitting this measure we can obtain the value of the CTI. Finally, subtracting the last mean measure of the peak, from the mean signal of the peak at the first column, we can know the number of electrons lost.

3.3 Short comment on the results

As explained above, the LBNL wafers have four $4k \times 2k$, one $2k \times 2k$, and four $1k \times 0.5k$ pixels, and only the two bigger types will be used for DECam. Then, the little ones are produced, but are only used for testing and to gain experience in manipulating CCDs. As a test station has been developed in IFAE, some of the $1k \times 0.5k$ CCDs were sent from FNAL to IFAE in order to test them at The Slab.

During the test phase, the CCDs, have been damaged by several reasons, mostly due to storage (lack of humidity control) and improper handling. A new rack with humidity and temperature controllers, is now being built in the IFAE mechanical workshop.

We also had other problems. The Acquisition board (ACQ) that we used in The SLAB, seems to have an unknown source of noise. This is now being studied in order to solve the problem or to produce another board.

Finally, we have been testing the CCDs we had, and as a result many problems have been solved and many questions have been answered. Once the training has been done, now we are able to be a serious CCD characterization station, and we are now prepared to receive bigger CCDs.

Chapter 4

Conclusions

The Dark Energy Survey will employ four complementary techniques to study dark energy: galaxy clusters, weak lensing, galaxy angular clustering, and supernova distances. Combining these four probes, DES wants to determine the parameter w of the dark energy equation of state with a statistical precision of about 5%. For this, the DES will employ DECam, a powerful new wide-field survey instrument, and the Blanco, a 4 m telescope that has already contributed to many of the pioneering measurements of dark energy. At the focal plane of the DECam there will be sixty-two CCDs designed and developed at LBNL. The peculiarity of these CCDs is that they are more sensitive at near-infrared wavelengths due to their thickness (250 μm), achieving QE at 1000 nm of 60%.

To make sure that these CCDs accomplish the DES requirements, we have developed a test station in the IFAE laboratory, the SLAB. In it, there are all the instruments needed to perform a set of tests in order to characterize the behavior of the DES CCDs. The light emitted by a Xe lamp, is focused by an optical lens system, before passing through a filter that selects a determinate range of wavelengths. Then, a monochromator selects a narrow range, that enters into an integrating sphere. At 13 inches from the output port of this sphere, the DES cube is placed, which contains the CCD in a 10^{-6} mbar vacuum and at 173 K. These devices has been tuned separately in order to understand their response and to get the maximum profit from them.

The tests determine some parameters related to each of the functions the CCD can perform: charge generation, charge collection, charge transfer, and charge measurement. A CCD must pass all the tests separately to be classified as useful for scientific purposes. We used the previous system to illuminate the CCD surface, and varying the voltages applied on the CCD, we can check the different behavior of the CCDs.

With the accumulated experience and after fixing storage and handling issues that have damaged the CCDs, we should be capable of performing complete tests on the DES CCDs.

Appendix A

Error calculation

A.1 OTG and VOTGSCAN tests

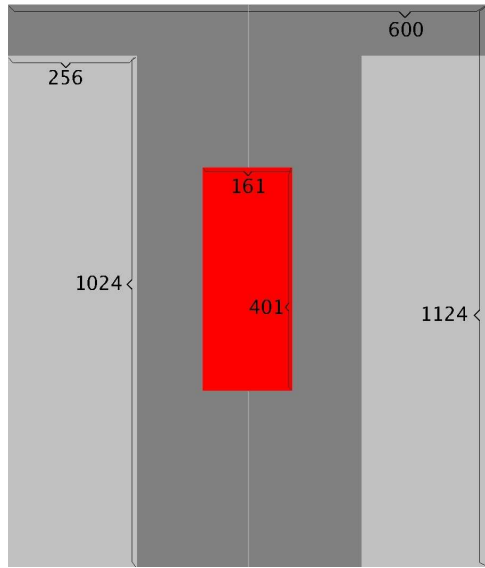


Figure A.1: Scheme of the regions in pixels of an output image. In light grey we see regions exposed to the light. In dark grey, the called overscan regions, they are the overclocks done in order to measure the signal generated without exposure. The red region is used to perform the OTG and VOTGSCAN tests.

In these two tests the same technique is used in order to measure when the charge injection occurs. The OTG test consists of 140 images, a clear and a 20 seconds exposure image, for each pair of values: V_{REF} , from -12 to -6 V, and V_{OTG} , from 0 to 9V, increasing 1 V each time. The VOTGSCAN test consists of 202 images, also a clear one and another exposed to the light during 20 seconds, but fixing V_{REF} at -12 V and scanning V_{OTG} from 0 to 10 V, increasing 0.1 V each time. The region of the images used to perform both the OTG and VOTGSCAN tests is shown in figure A.1. The mean signal value of the overscan region ($\hat{\mu}$) is measured separately

for each channel, using 401 rows and 161 columns. The formulas used are

$$\hat{\mu} = \frac{\sum x_i}{N} \quad (\text{A.1})$$

$$\sigma^2 = \frac{\sum (x_i - \hat{\mu})^2}{N-1} \quad (\text{A.2})$$

$$\Delta\hat{\mu} = \frac{\sigma}{\sqrt{N}} \quad (\text{A.3})$$

where x_i is the signal of the i pixel, and N the number of pixels of the overscan region used to measure the mean. In both tests, the mean value and its error is plotted as a function of the respective voltages.

A.2 PTC test

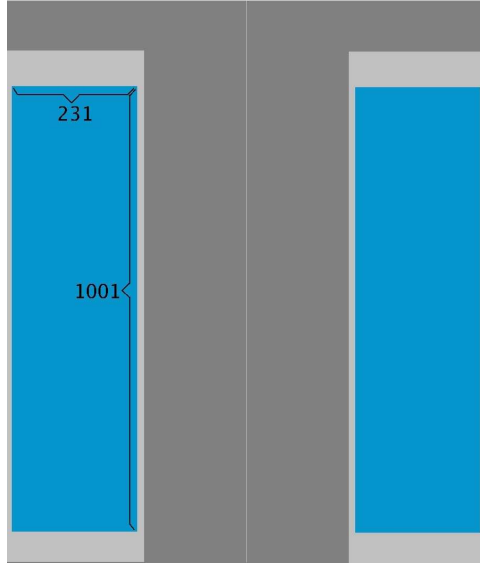


Figure A.2: The blue region corresponds to the region used to perform the PTC test.

In this tests 320 images are taken, eight for each exposure time from 1 to 40 seconds increasing 1 second each time. For each exposure time the following sequence takes place twice: a clear image, a not exposed to the light image (NOTEXP), another clear image, and a light exposed image (EXP). The clear images are not used anymore. The areas of the images used for the analysis are shown in figure A.2.

From the 231-column wide and 1001-row tall selected region from each channel, three mean values are measured: the mean value of the two EXP images ($\hat{\mu}_{EXP}$), the mean value of the NOTEXP ones ($\hat{\mu}_{NOTEXP}$), and the mean value of the subtraction of the previous mean values

$(\hat{\mu}_{DIFF})$. Each measurement is performed pixel by pixel

$$\bar{x}_i = \frac{x_{i1} + x_{i2}}{2} \quad (\text{A.4})$$

$$\hat{\mu} = \frac{\sum \bar{x}_i}{N} \quad (\text{A.5})$$

$$\sigma_{\mu}^2 = \frac{\sum (\bar{x}_i - \hat{\mu})^2}{N - 1} \quad (\text{A.6})$$

$$\Delta\hat{\mu} = \frac{\sigma_{\mu}}{\sqrt{N}} \quad (\text{A.7})$$

where \bar{x}_i is the mean signal of the pixel i , N the number of pixels scanned, and $\hat{\mu}$ the mean value of the region scanned.

The three mean values are plotted as a function of the exposure time. In this plot, linear fits are performed for each mean value separately. The non-linearity is measured subtracting the DIFF mean signal value from the linear fit.

$$NLT_i = \frac{\hat{\mu}_i}{p_0 + t_i p_1} - 1 < 0.01 \quad \forall i \quad (\text{A.8})$$

$$\sigma_{NLT_i}^2 = \frac{1}{(p_0 + t_i p_1)^2} \left[\Delta\hat{\mu}^2 + \left(\frac{\hat{\mu}_i}{p_0 + t_i p_1} \right)^2 \Delta p_0^2 + \left(\frac{\hat{\mu}_i t_i}{p_0 + t_i p_1} \right)^2 \Delta p_1^2 \right] \quad (\text{A.9})$$

where p_0 and p_1 are the parameters of the fit, and t_i the exposure time.

For the calculation of the camera gain constant the variance is measured subtracting pixel by pixel the two EXP images:

$$\bar{x}_{i,r} = x_{i1} - x_{i2} \quad (\text{A.10})$$

Then the mean value of the subtraction is measured.

$$\hat{\mu}_r = \frac{\sum \bar{x}_{i,r}}{N} \quad (\text{A.11})$$

$$\sigma_{\hat{\mu}_r}^2 = \frac{\sum (\bar{x}_{i,r} - \hat{\mu}_r)^2}{N - 1} \quad (\text{A.12})$$

$$\Delta\sigma_{\hat{\mu}_r}^2 = \frac{\sigma_{\hat{\mu}_r}}{\sqrt{2N}} \quad (\text{A.13})$$

Another measure of the variance is done supposing that the mean value of the subtraction of the two EXP images is zero.

$$\sigma_r^2 = \frac{\sum (\bar{x}_{i,r} - \mu)^2}{N - 1} \quad \text{with } \mu = 0 \quad (\text{A.14})$$

$$\Delta\sigma_r^2 = \frac{\sigma_r}{\sqrt{2N}} \quad (\text{A.15})$$

The two variance measurements are plotted as a function of the mean EXP value, for each exposure time.

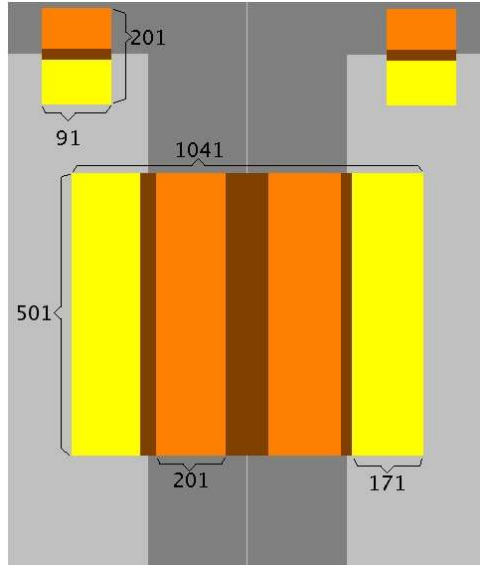


Figure A.3: Region of the images used to perform the CTI test. The two top regions are used to measure the vertical voltages, and the central region to measure the horizontal ones. In the horizontal study, all the colored region is used to measure the mean signal per columns ($\hat{\mu}_i$), the yellow region to measure the mean value of the exposed area ($\hat{\mu}_{MEAN}$), and the orange to measure the pedestal ($\hat{\mu}_{PED}$). In the vertical study the same measurements are performed but in rows.

A.3 CTI test

In the CTI test, four kinds of studies are done, fixing three of the four transfer voltages and varying the other: $V+, H+$, are scanned from 0 to 10V, and $V-, H-$, from -10 to 0V, increasing 0.5 V each time. For each scanned voltage a clear and a 10 second exposed image are taken. Finally, a total of 160 images are taken, 40 per voltage value. The regions used to perform this test are shown in figure A.3.

In the study of the horizontal voltages, the column signal mean (COL) is computed from a region of 1041 columns and 501 rows from the exposed images, containing the transition from exposed area to overscan. From this region, 171 columns are used to measure the mean value of the exposed area (MEAN), and 201 for the measurement of the pedestal in the overscan region (PED), in each channel separately. In the vertical voltage study, two regions of 90 columns and 201 rows are selected, and the same three parameters are measured but in rows.

For the COL measurement we use the typical mean and variance equations,

$$\hat{\mu}_i = \frac{\sum x_i}{N_i} \quad (A.16)$$

$$\sigma_i^2 = \frac{\sum (x_i - \hat{\mu}_i)^2}{N_i - 1} \quad (A.17)$$

$$\Delta \hat{\mu}_i = \frac{\sigma_i}{\sqrt{N_i}} \quad (A.18)$$

where x_i is the signal value of each pixel in column i , and N_i is the number of pixels scanned in column i , in our case 401.

For the MEAN and PED measurement we use the same equations,

$$\hat{\mu}_l = \frac{\sum x_i}{N_l} \quad (\text{A.19})$$

$$\sigma_l^2 = \frac{\sum(x_i - \hat{\mu}_l)^2}{N_l - 1} \quad (\text{A.20})$$

$$\Delta\hat{\mu}_l = \frac{\sigma_l}{\sqrt{N_l}} \quad (\text{A.21})$$

where l can be referred to MEAN or PED, $x_{i,l}$ is the value of the pixel i involved in each measurement, and N_l is the number of pixels used in each measurement. Recall that once these measurements are done, we have i values of $\hat{\mu}_i$, and only one of $\hat{\mu}_{MEAN}$ and one of $\hat{\mu}_{PED}$.

The normalized mean value of each column is measured dividing the mean signal of each column after subtracting the pedestal, by the mean exposed area signal after subtracting the pedestal.

$$sig_i = \frac{\hat{\mu}_i - \hat{\mu}_{PED}}{\hat{\mu}_{MEAN} - \hat{\mu}_{PED}} \quad (\text{A.22})$$

$$\sigma_{sig_i}^2 = \frac{1}{(\hat{\mu}_{MEAN} - \hat{\mu}_{PED})^2} [\Delta\hat{\mu}_i^2 + (sig_i - 1)^2 \Delta\hat{\mu}_{PED}^2 + sig_i^2 \Delta\hat{\mu}_{MEAN}^2] \quad (\text{A.23})$$

This normalized mean value is then plotted as a function of column number. In the definition of sig_i , there is any problem with singularities because always $\hat{\mu}_{MEAN} > \hat{\mu}_{PED}$.

The charge transfer inefficiency is measured dividing the normalized mean signal of the last column of the overscan region before the exposed region, by the number of transfers required to move its original charge to the readout gate.

$$CTI = \frac{sig_{last}}{N_{transfers}} \quad (\text{A.24})$$

$$\Delta CTI = \left(\frac{\partial CTI}{\partial sig_{last}} \right)^2 \Delta sig^2 = \frac{\Delta sig_{last}^2}{N_{transfers}^2} \quad (\text{A.25})$$

where $N_{transfers}$ is 256 in our case. The CTI is plotted as a function of the scanned voltage value.

Appendix B

Full test example

CCD Testing Report

Device ID	pb-512-19
Type	Back Illuminated
Size	1024x512
Thickness	250 μm
Operator	Lluis Galbany
Analysis	Lluis Galbany

Results Analysis:

	Right Amp. (RH)	Left Amp. (LH)
Gain (ADU/e)	1.223 ± 0.000	3.118 ± 0.000
Noise (ADU)	12.410 ± 0.023	11.267 ± 0.020
Full Well Capacity(e)	~ 180000	~ 180000
Nonlinearity > 1% (s)	12 ± 1	9 ± 1
Output Gate for Charge Inj. Vref=-12V (V)	2.6 ± 0.1	2.1 ± 0.1
Minimal H+ for CTI requirements (V)	5.5 ± 0.5	6.0 ± 0.5
Minimal H- for CTI requirements (V)	-10.0 ± 0.5	-10.0 ± 0.5
Minimal V+ for CTI requirements (V)	1.0 ± 0.5	1.0 ± 0.5
Minimal V- for CTI requirements (V)	-10.0 ± 0.5	-10.0 ± 0.5
CTI calculus from Fe^{55} source	$3.13 \cdot 10^{-6}$	$4.01 \cdot 10^{-7}$

B.1 OTG

This test is done in order to see at which voltage of V_{OTG} the charge injection into the CCD takes place. The scan in values of V_{OTG} is done for various values of V_{REF} .

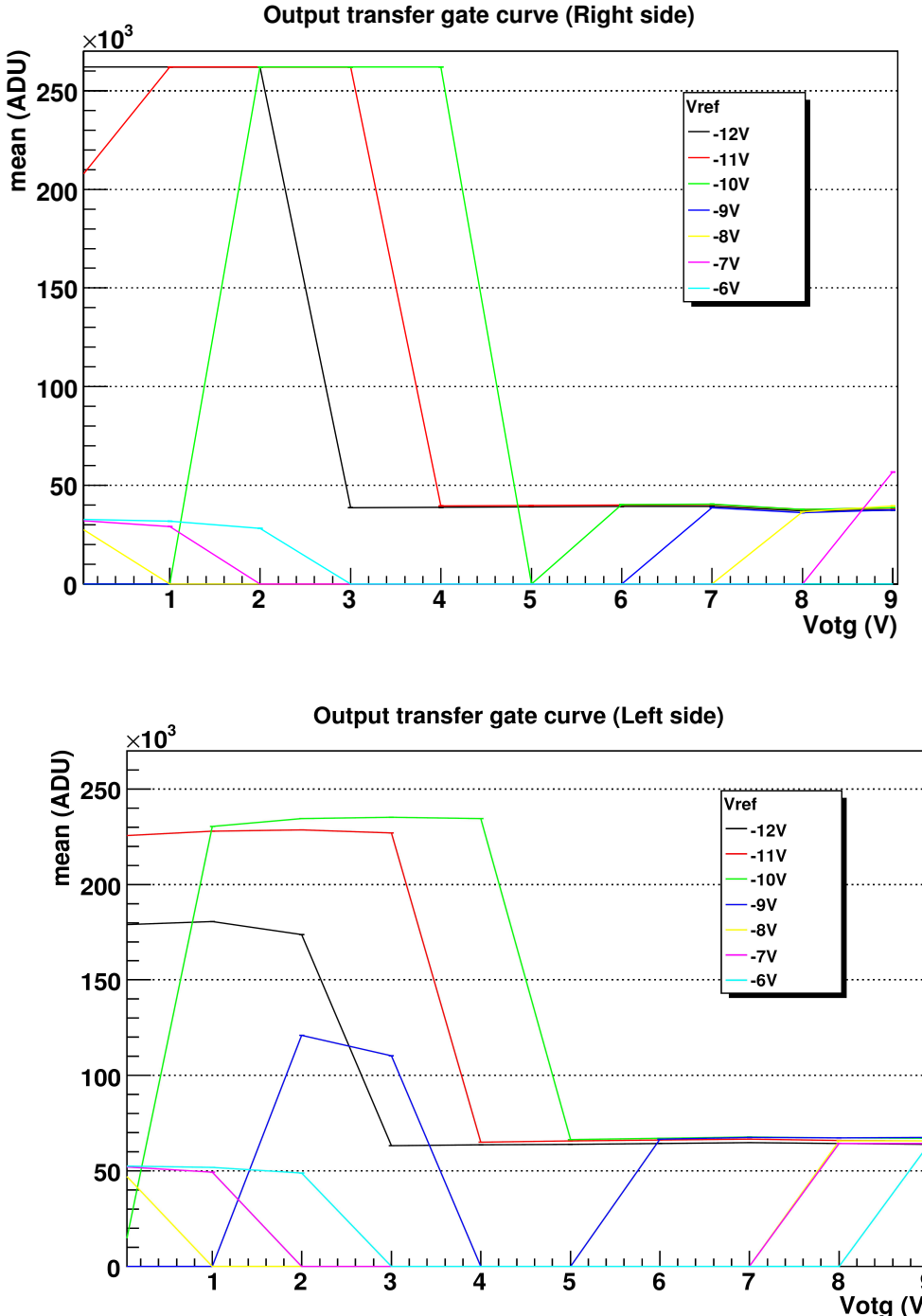


Figure B.1: Each point is an image. The mean in the overscan region is plotted as a function of V_{OTG} for different values of V_{REF} . On the top for the right amplifier, and on the bottom for the left amplifier.

B.2 VOTGSCAN

This test is done to see more exactly at which value of V_{OTG} the charge injection occurs. V_{REF} is fixed at 12 V and the scan in V_{OTG} is made increasing 0.1 V in each image.

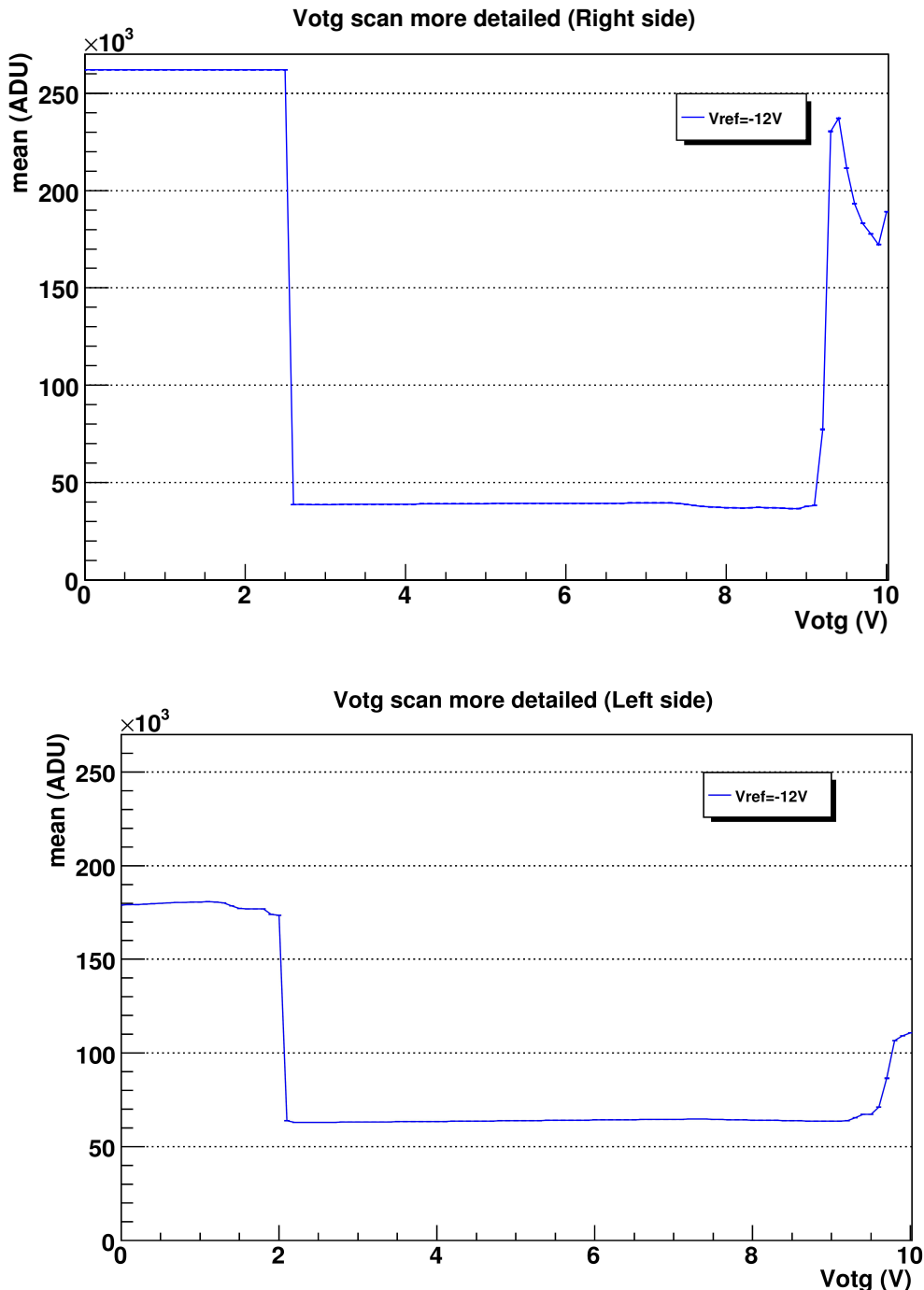


Figure B.2: The same kind of images as in OTG test but fixing V_{REF} at 12 V and varying V_{OTG} 0.1 V, from 0 to 9.5 V. On the top for the right amplifier, and on the bottom for the left amplifier.

B.3 PTC

Light exposed images from 1 to 40 sec are taken in order to measure the full-well potential, the linearity of the charge generation with time, the dark current, the pedestal, and the camera gain constant.

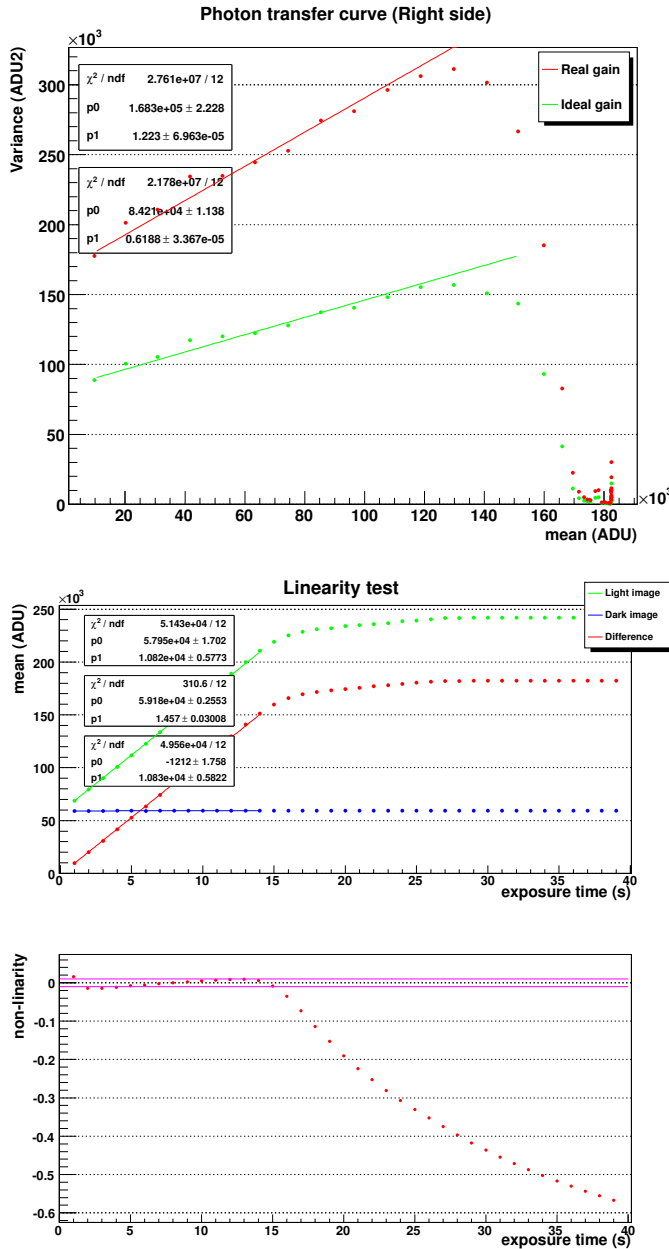


Figure B.3: Top: Photon transfer curve for the right amplifier. The linear fit corresponds to the camera gain constant. The points converge to the full-well potential. Middle: Mean signal as a function of exposure time. The intersection between the green fit and the y-axis corresponds to the pedestal. The blue points are a measure of dark current. Bottom: The fractional difference between the linear fit and the data in the middle panel.

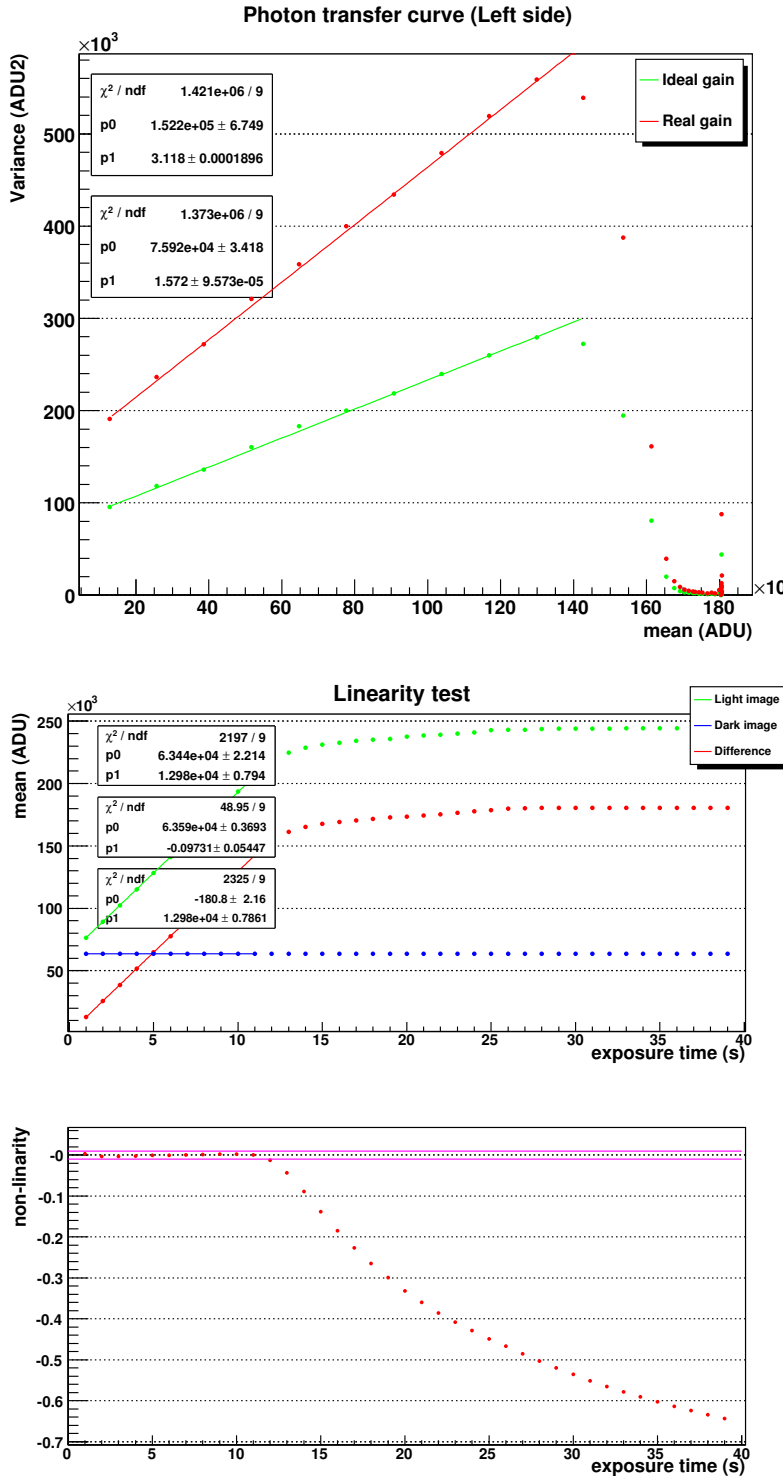


Figure B.4: Top: Photon transfer curve for the left amplifier. The linear fit corresponds to the camera gain constant. The points converge to the full-well potential. Middle: Mean signal as a function of exposure time. The intersection between the green fit and the y-axis corresponds to the pedestal. The blue points are a measure of dark current. Bottom: The fractional difference between the linear fit and the data in the middle panel.

B.4 CTI

This test is done in order to make a measurement of the charge transfer inefficiency. In the different studies one of the voltages is changed while the others are left at the operating values.

B.4.1 H+

The transition between the exposed area to the overscan region for the right amplifier. The mean per columns is calculated and, after subtracting the pedestal and normalizing to the exposed mean signal, plotted per columns. The CTI is measured dividing the signal of the first non-illuminated column by the number of transfers from this last column to the readout gate.

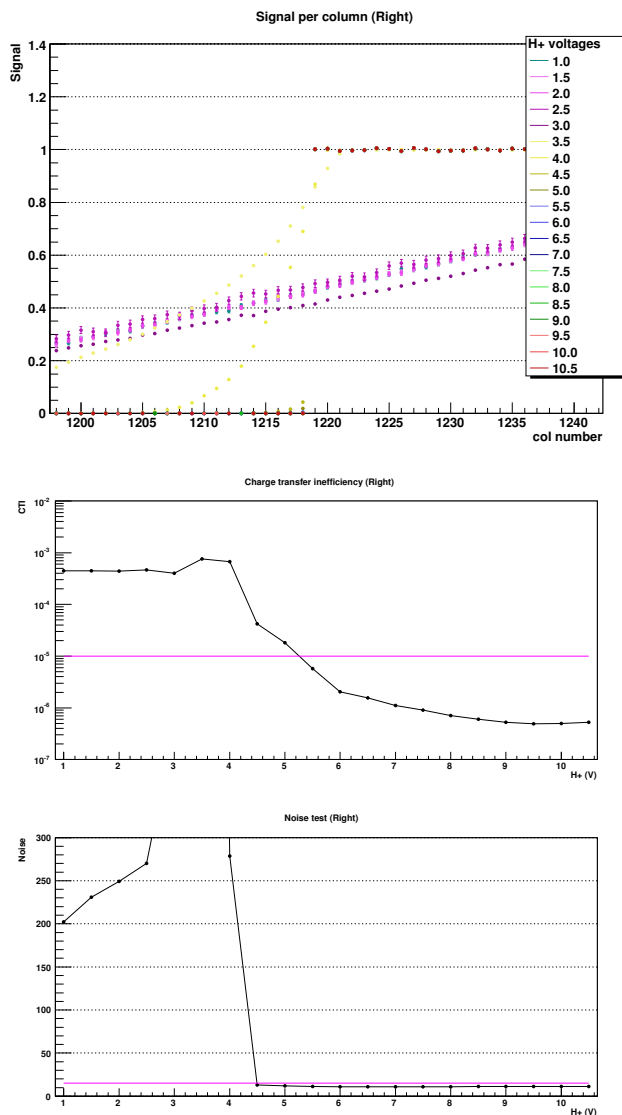


Figure B.5: Top: Transition from the exposed area to the overscan region for the right amplifier. Middle: Charge transfer inefficiency as a function of H^+ voltage. Bottom: Noise as a function of the H^+ voltage.

The result is also shown for the left amplifier. The CTI as a function of the H⁺ voltage is also plotted. At some voltage the DES requirement is achieved. The noise for every image is measured in order to see how it changes.

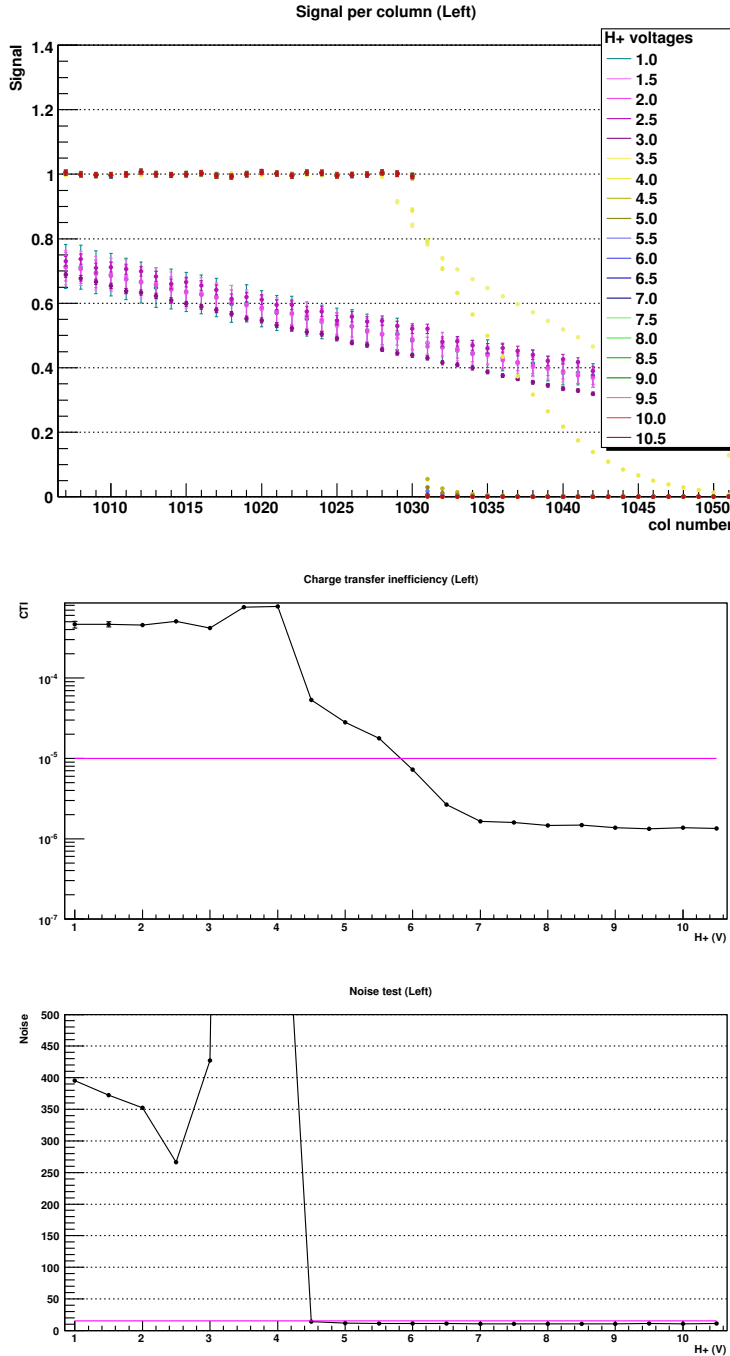


Figure B.6: Top: Transition from the exposed area to the overscan region for the left amplifier. Middle: Charge transfer inefficiency as a function of H⁺ voltage. Bottom: Noise as a function of the H⁺ voltage.

B.4.2 H-

The same measures than previously but fixing H+ and varying H-, for the right amplifier.

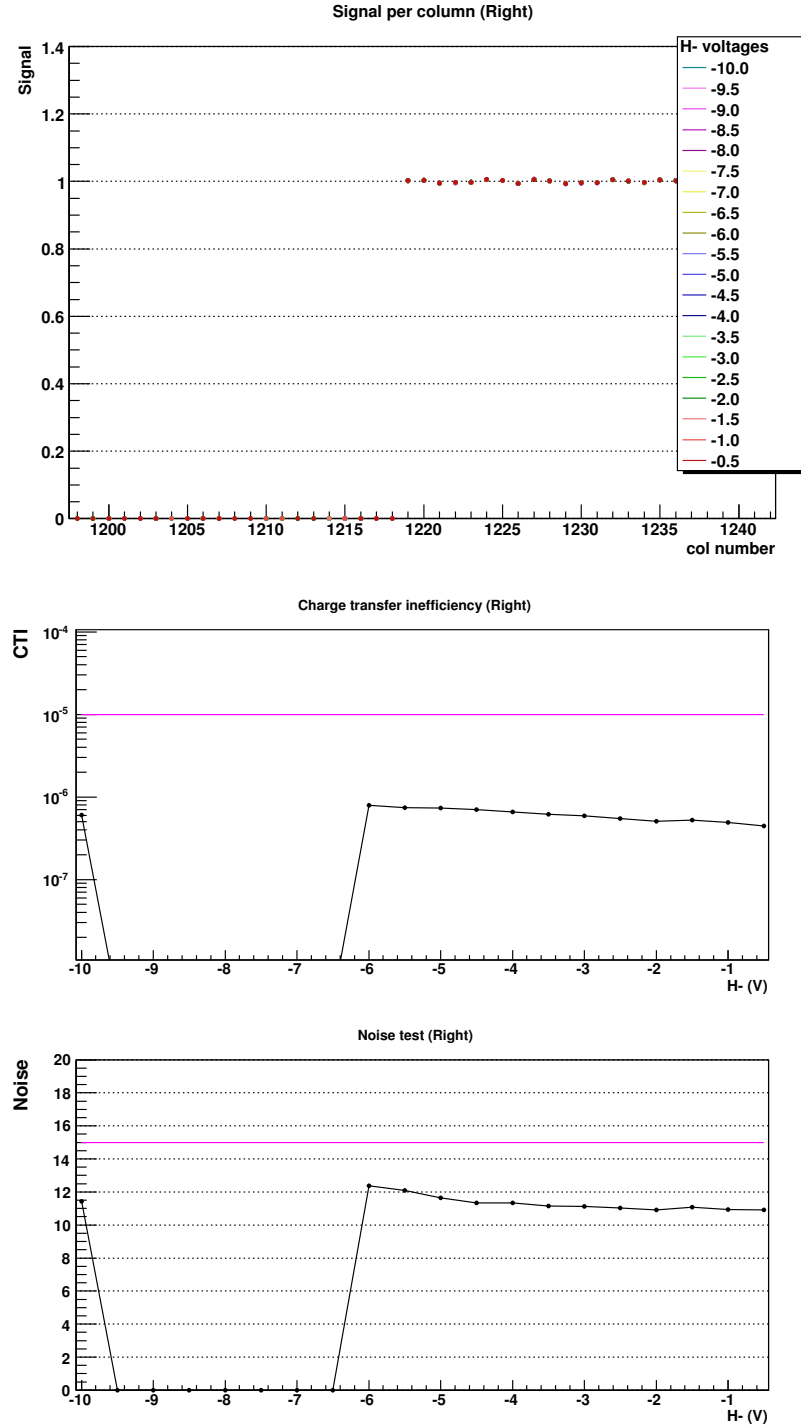


Figure B.7: Top: Transition from the exposed area to the overscan region for the right amplifier. Middle: Charge transfer inefficiency as a function of H- voltage. Bottom: Noise as a function of the H- voltage.

And also for the left amplifier.

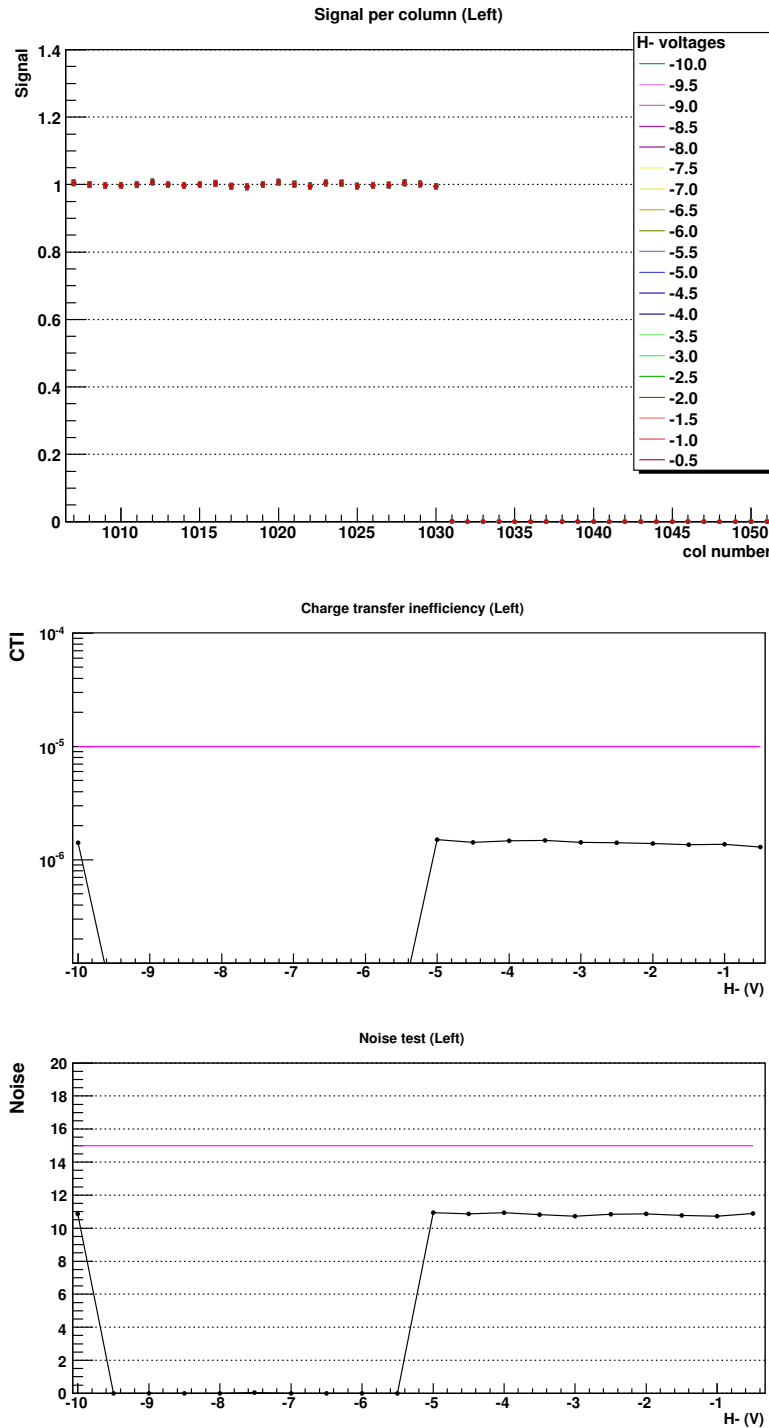


Figure B.8: Top: Transition from the exposed area to the overscan region for the left amplifier. Middle: Charge transfer inefficiency as a function of H^- voltage. Bottom: Noise as a function of the H^- voltage.

B.4.3 V+

In this case the charge transfer inefficiency is measured using the vertical overscan region, for the right amplifier. The V+ voltage is varied fixing the other transfer voltages. The CTI is measured dividing the signal mean of the first row of the overscan region by the number of vertical transfers to the horizontal serial register.

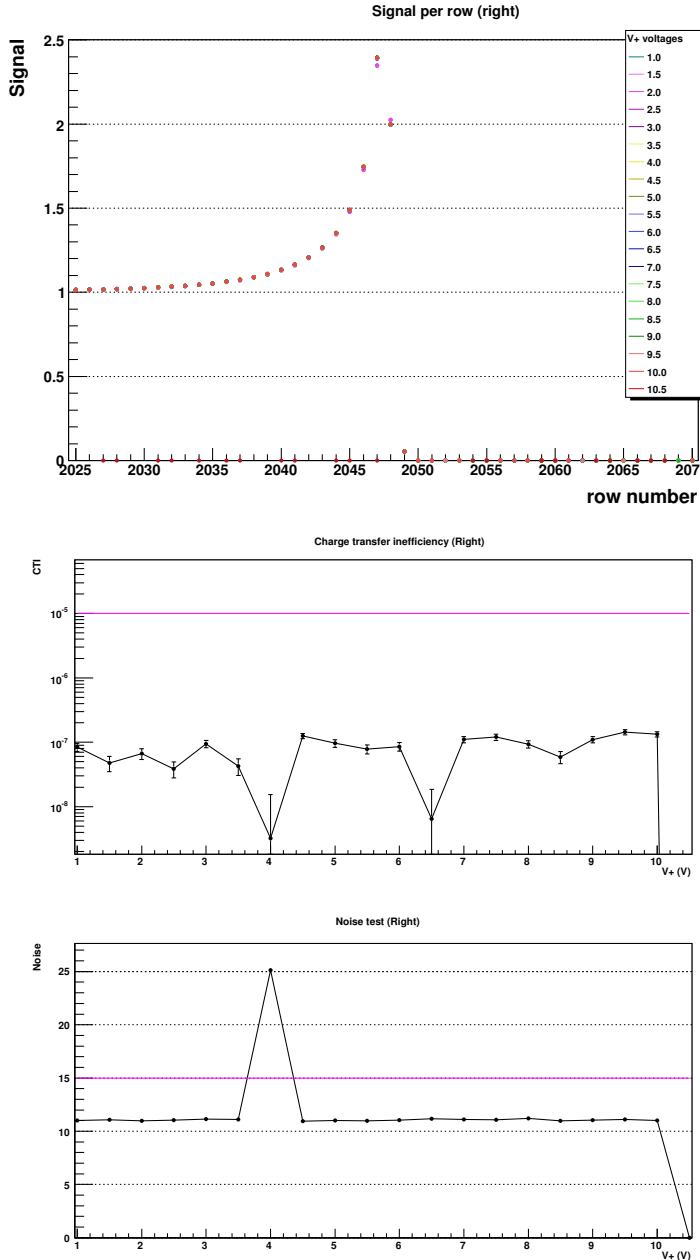


Figure B.9: Top: Transition from the exposed area to the overscan region for the right amplifier. Middle: Charge transfer inefficiency as a function of V+ voltage. Bottom: Noise as a function of the V+ voltage.

Also for the left amplifier.

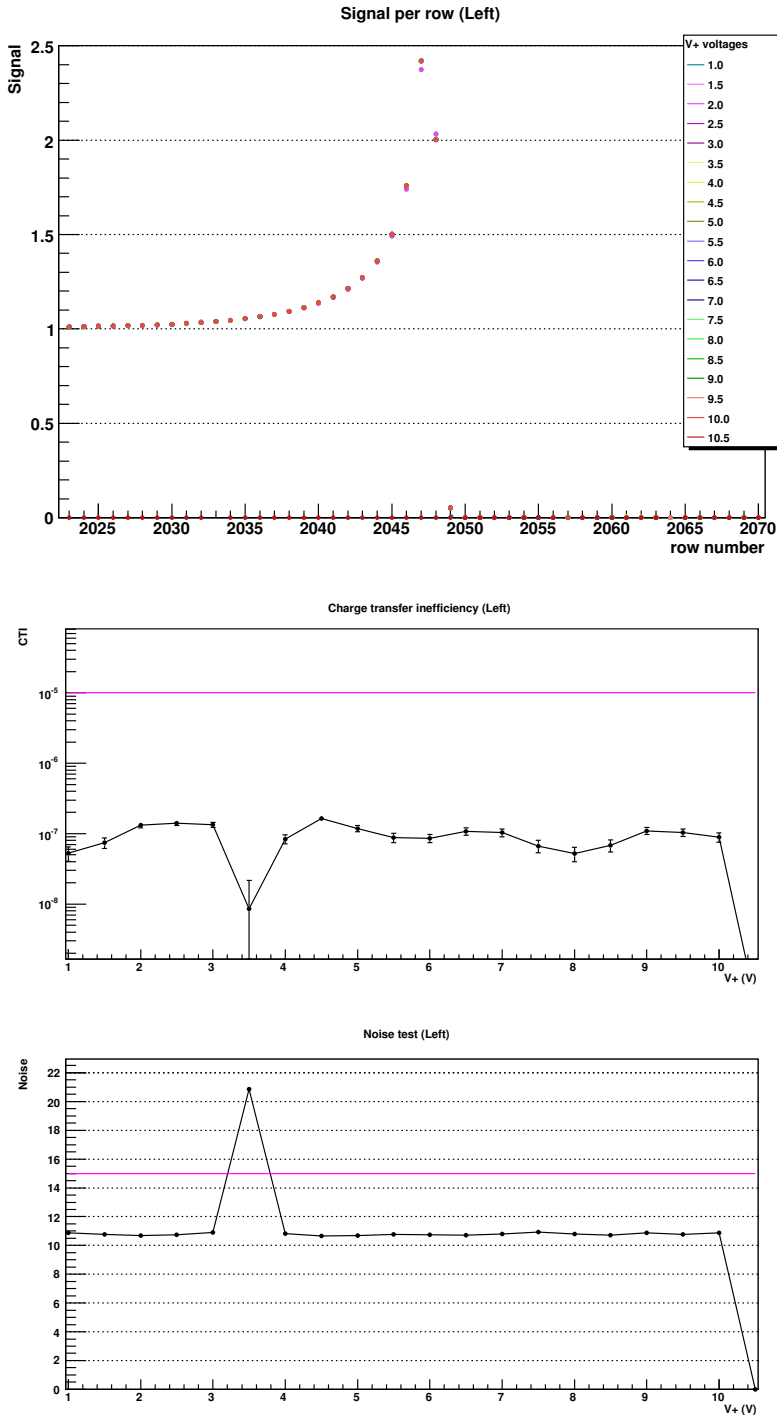


Figure B.10: Top: Transition from the exposed area to the overscan region for the left amplifier. Middle: Charge transfer inefficiency as a function of V_+ voltage. Bottom: Noise as a function of the V_+ voltage.

B.4.4 V-

The same measurements as before but fixing V+ and varying V-, for the right amplifier.

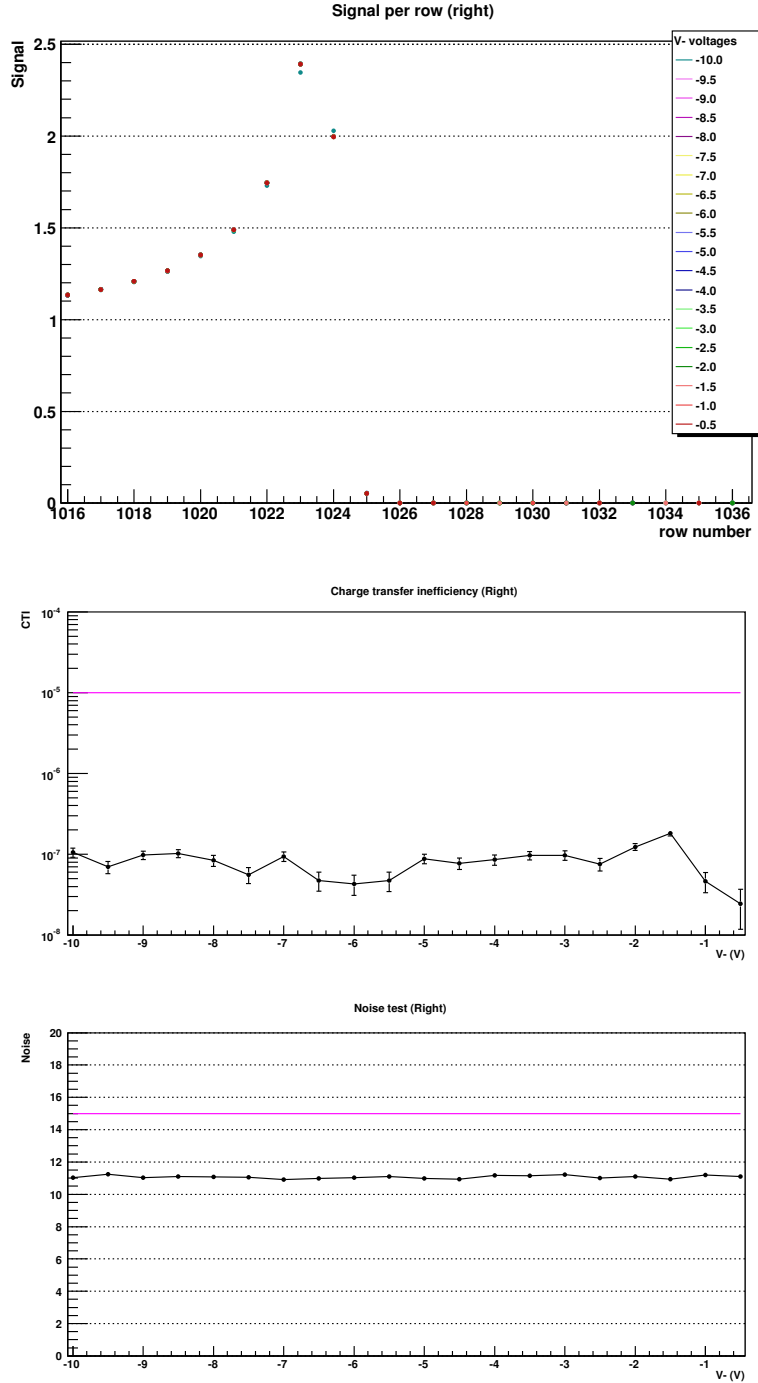


Figure B.11: Transition between the parallel overscan in the right to the exposed area in the left. The different colors correspond to different values of V-. Top: Vertical CTI as a function of V-. Bottom: Measured noise as a function of V-.

And also for the left amplifier.

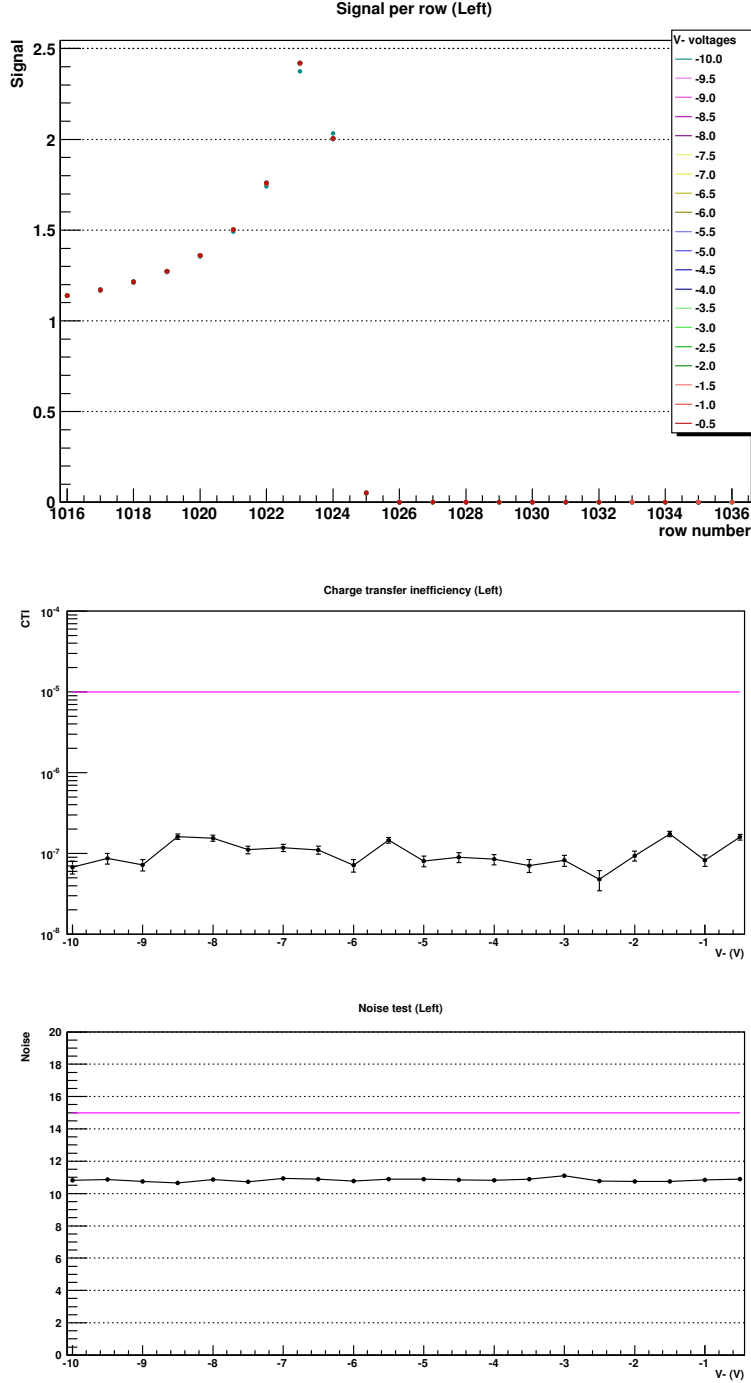


Figure B.12: Transition between the parallel overscan in the right to the exposed area in the left. The different colors correspond to different values of V_- . Top: Vertical CTI as a function of V_- . Bottom: Measured noise as a function of V_- .

B.5 NOISE

This test is done averaging ten images exposed to the light for about 10 seconds, and plotting the signal of all the pixels in a histogram. The rms is equal to the noise.

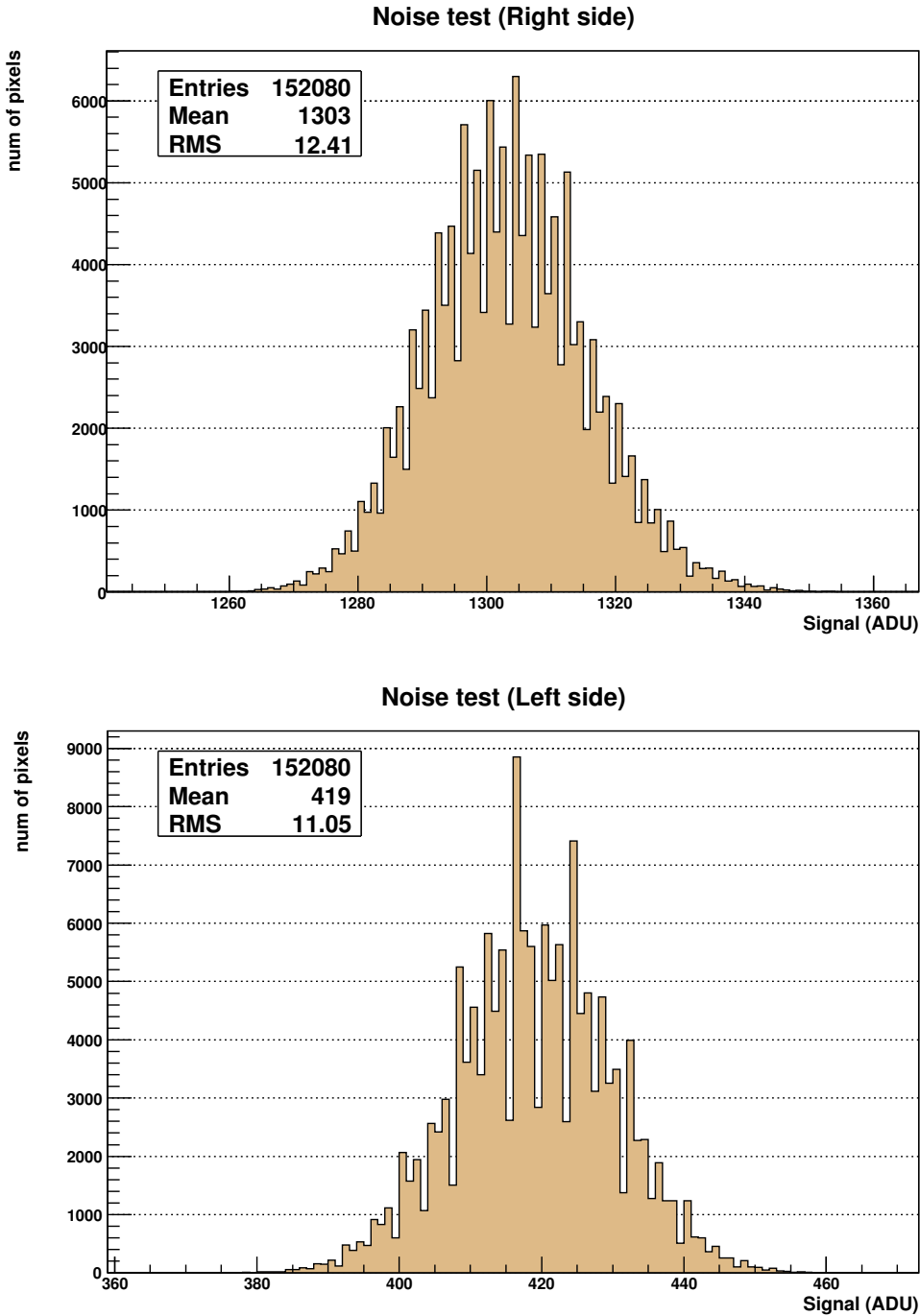


Figure B.13: Top: NOISE test for the right amplifier, Bottom: For the left amplifier.

B.6 X-Ray exposure

This is a measurement of the charge transfer inefficiency by exposing the CCD to a ^{55}Fe X-ray source. The pixel signal distribution is plotted, and the CTI is measured taking the mean value of the K_{α} peak every fifty columns, and fitting these points.

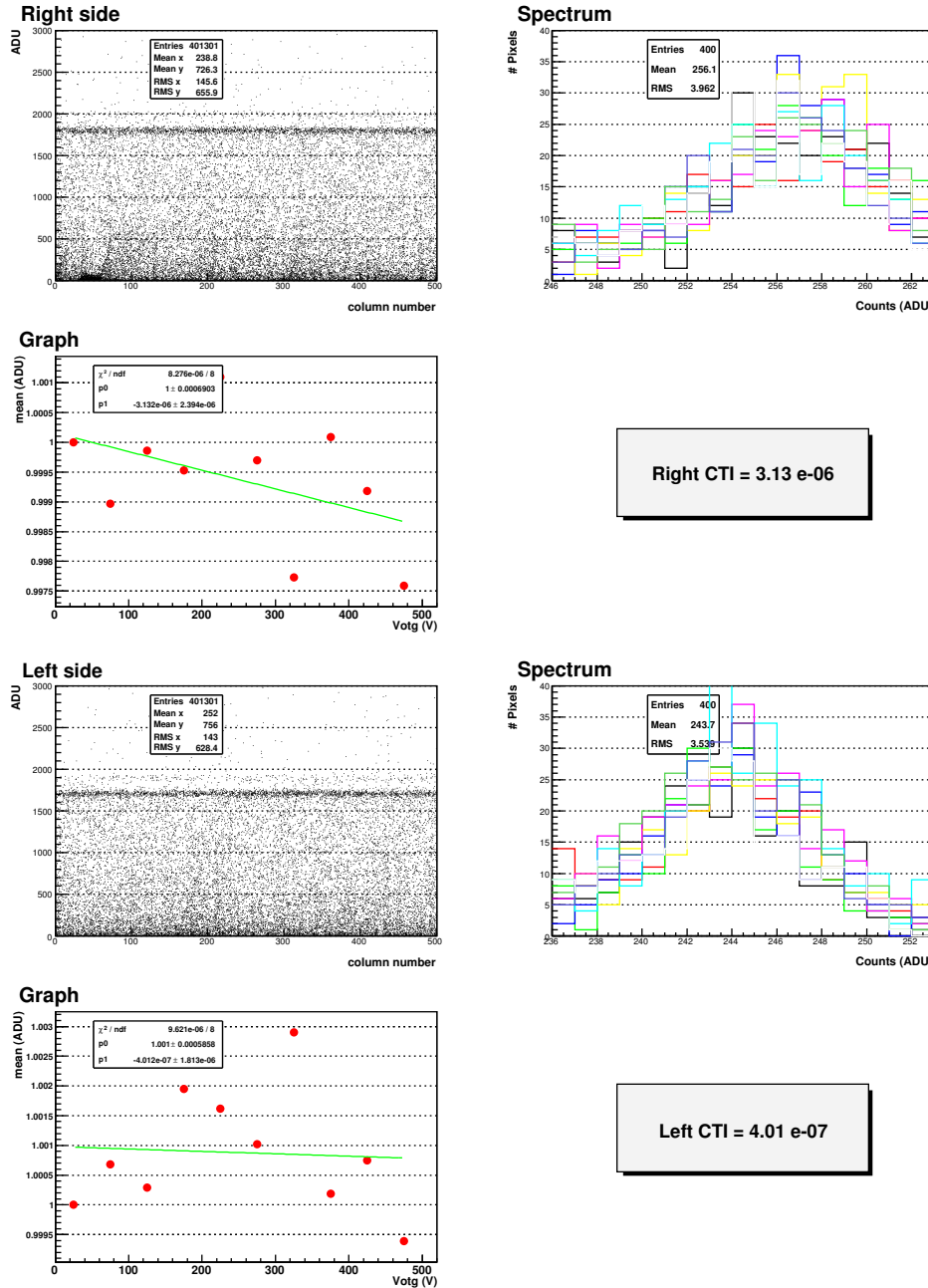


Figure B.14: Top left: The pixel signal distribution per columns. Top right: The K_{α} peak measured from every fifty columns. Bottom left: The fit of the mean value of the K_{α} every 50 columns as a function of the column number.

Bibliography

- [1] Fukigita, M., et al, 1996, AJ, 111, 1748
- [2] Riess, A., et al. 1998, AJ, 116, 1009e
- [3] Perlmutter, S., et al. 1999, ApJ, 517, 565
- [4] Hubble webpage, <http://hubblesite.org/gallery/>
- [5] Ruhl, J., et al 2004, in Astronomical Structures and Mechanisms Technology, edited by Antebi, J. & Lemke, D., Proc. SPIE, 5498, 11; astro-ph/0411122
- [6] Hu, W. 2002, Phys. Rev. D, 66, 083515
- [7] Huterer, D. 2002, Phys. Rev. D, 65, 063001
- [8] Phillips, M. M. 1993, ApJ, 413, L105
- [9] Eisenstein, D. J., et al. 2005, ApJ, submitted, astro-ph/0501171
- [10] Hu, W., & Scranton, R. 2004, Phys. Rev. D, 70, 123002
- [11] Holland, S. E., et al. 2003, IEEE Trans. Electron Dev., 50(3), 225
- [12] Integrating Sphere Uniform Light Source Applications, Labsphere tech guide
- [13] DES-Spain wiki site, <http://deswiki.ifae.es>
- [14] Serrano, S., Instrument control software manual, DES-Spain
- [15] Yao, W-M., et al., Journal of Physics, G 33, 1 (2006) (p. 284)
- [16] Janesick, J. R., Scientific Charge Coupled Devices, SPIE Press